DESIGN OF MACHINES AND STRUCTURES

A Publication of the University of Miskolc

Volume 6, Number 2 (2016)

CONTENTS

ON MODELLING OF SURFACE NANOPATTERN EVOLUTION PROCESSES

GABRIELLA BOGNÁR

University of Miskolc, Institute of Machine and Product Design
3515 Miskolc-Egyetemváros
v.bognar.gabriella@uni-miskolc.hu

Abstract: First we review different models of surface growth processes. Then we focus on the calculation of the surface roughness for the amorphous thin film growth represented by a one-dimensional deterministic field equation. On the base of numerical simulations, better understanding of the amorphous thin film growth process is available. The temporal evolution of the surface roughness of the surface morphology with parameter data has been presented. The effect of the parameter is significant on the height profile, on the mean average height profile and on the surface roughness.

Keywords: surface morphology, surface evolution, growth model, roughness

1. INTRODUCTION

Surface roughness has a huge impact on many important phenomena. Typical examples of spatiotemporal pattern formation in systems driven away from equilibrium can be found in physical, chemical and biological processes such as in hydrodynamic systems in pure fluids and mixtures, in patterns of solidification fronts, in optics, in chemical reactions and in excitable biological media [2]. While on micro- and macro scales one can control the processes by special devices, on nano scales such instruments are absent or their use is extremely expensive. Therefore, the investigation of self-organization and self-assembly provide promising mode to understand basic physical principles and mechanisms. The understanding of these processes can allow us to extend the use of such technique to a large variety of fabrication processes, to create new electronic devices, sensors and tailored surfaces; moreover, to controllably modify chemico-physical properties of the surface by tailoring the nanoscale morphology during patterning and to optimize certain film properties like roughness and coarsening.

In many industrial applications a thin film of a solid material needs to be deposited on a solid semiconductor substrate. This deposition can be made by different methods, e.g., by ion beam sputtering, Physical Vapour Deposition (PVD) or Chemical Vapour Deposition (CVD), and during the growth process atoms of the film stick to the atoms of the substrate at its surface. Usually, the growing film does not remain planar during its growth and various kinds of surface structures are

developed. The types of these structures depend on physical characteristics of the materials as well as on the growth conditions.

The main objective is to introduce deterministic equations that describe physical phenomena and their solutions are most likely received from the initial condition and will remain valid even after a long time.

Surfaces can be smooth but the same surface can also be rough. Surfaces with "ideal" topography, e.g., prepared by fracture or by some growth process, have been studied intensively for many years [2–6, 8]. An important question is how we can describe the morphology and how to study surface and interface dynamics.

2. TOOLS

In the mathematical approach, it is important to incorporate the uncertainty of the parameters into the model. The main sources of uncertainties are difficult to predict. These include the elastic interaction at atomic level, surface state changes and others. The irregular surfaces are characterized by partial differential equations together with free boundary conditions. To find analytical solution to these partial differential equations is usually impossible, the applied numerical algorithms are generally unstable, and therefore variation methods have to be used. With this approach, the singular geometries can also be treated.

The theoretical base is the system of partial differential equations. The deterministic equations of motion are usually non-linear differential equations. They are sometimes supplemented by stochastic members, which represent temperature or instrumental noises. In carefully designed experiments on macro scale stochastic forces are negligible. Some aspects of self-assembly of quantum dots in thin solid films are considered. Nonlinear evolution equations describing the dynamics of the film instability that results in various surface nanostructures are analyzed in the literature [9–16]. Pattern formation is analyzed by means of amplitude equations.

Reports on the production of submicron and nanometric patterns on the surfaces of solid targets eroded by ion irradiation are dated back to the 1960s. In 1956 NAVEZ et al. [19] observed the phenomenon, that bombarding a glass surface with an ion beam of air, the bombardment produced a new morphology depending mainly on the incidence angle θ of the ion beam. The obtained surface is covered by wavelike structures (ripples) separated by distances ranging from 30 to 120 nm. The authors tried to find analogies with macroscopic phenomena such as the ripple structures formed by wind over a sand bed. The observed formations in sand dunes and in clouds are very similar to the features observed on the glass modified by ion bombardment [22] when air and sand come into contact, as they can be considered as two immiscible fluids. Air and sand can be moving at very different speeds. The boundary between them can develop complex wavelike structures and ripples. The morphologies of sand dunes are qualitatively similar to that obtained by sandblasting. The same experiment as in [18] compared with sand ripples observed in the desert in paper [23].

One of the typical features of quantum dots is that they formed spontaneously due to the instability of a thin solid film deposited on a solid substrate. Therefore, one can talk about self-assembly of quantum dots. The self-assembled quantum dots can have various shapes: regular, as faceted pyramids; irregular, as small crystals with many facets in various orientations; rounded, as cones [12].

When an array of quantum dots formed on the surface of a solid film is kept at a fixed temperature, the dots can either exhibit coarsening or not. During coarsening the larger dots grow at the expense of the smaller ones so that the average dot size increases in time. In the absence of coarsening, the dot size distribution does not essentially evolve at all. The mechanisms that govern the shape of quantum dots, the dynamics of their formation and the evolution of the quantum dot arrays are expressed in several models.

The principal mechanisms that govern the formation, morphology and evolution of quantum dots are elastic stress, anisotropic surface energy and surface diffusion. Since the 1960s surface pattern formations have been found on the variety of materials. The periodicity of the ripples can be tuned by bombarding the surface with varying energy of ions (typically in the range of 0.1 to 100 keV). Depending on the angle of incidence of the ion beam the surface ripples can be oriented parallel or perpendicular or hexagonally ordered.

Surface-energy anisotropy is responsible for the equilibrium shape of a given material with a fixed volume which minimizes the total energy of its surface. If the surface energy of the material is isotropic (that is a constant), the equilibrium shape must minimize the total surface area. When the volume is fixed this minimization is provided by a spherical shape. When the surface energy is anisotropic and depends on the surface orientation, a shape that minimizes the total surface energy, under the constraint of a fixed volume, is no longer spherical. It is given by a solution of a corresponding variational problem that leads to a nonlinear partial differential equation of the second order for the surface shape.

During the mechanism of instability of a thin solid film deposited on a solid substrate, the substrate can prescribe the film to grow in a specific orientation that would have been forbidden in the absence of the substrate. When the film becomes thick enough and does not "feel" the substrate any more it will undergo faceting instability and decompose into a system of faceted islands.

Theoretical predictions for surface structures are derived by partial differential equations involving the derivatives of a time dependent height function $h(x,y,t)$ of the surface, describing film growth at a mesoscopic level. Numerous conservative continuum equations have subsequently been proposed [13], since in many practical situations the dominant surface relaxation mechanism is surface diffusion, with vacancy formation and particle desorption being quite negligible. Usually such models admit main contributions related to both local dynamics, chemical reactions type of birth and deaths processes, and mass transport [15]. In testing the validity of the theory it is important to identify the right terms of the evolution equation.

(i)   The Edwards–Wilkinson (EW) model plays an important role in the study of non-equilibrium surface growth due to the simplicity of its growth process. A lattice model was introduced for the study of fluctuations in a surface, growing by random deposition of particles with immediate relaxation to nearest-neighbour sites. Based on the lattice model, Edwards and Wilkinson derived an equation which is purported to describe the surface fluctuations during growth. The EW equation is written as

$$h_t(x,t) = \nu \nabla^2 h + \eta(x,t),\tag{1}$$

where ν is the surface tension, and η is the stochastic contribution to the surface fluctuations.

It is important to note that the linear evolution *Equation (1)* is mathematically ill-posed, unbounded growth of short wavelength models appear.

(ii) The Kardar, Parisi and Zhang (KPZ) model [2], is a very well-known example of the growth process, suggested a continuum equation which does not conserve particle number, and is therefore applicable to cases where desorption and/or vacancy formation, but not surface diffusion, are the dominant surface relaxation mechanisms.

It was introduced in the context of studying the motion of growing interfaces for connections between polymers and lattice gases in [14]. Experimental observations caught the imagination are published for many applications. For example, physical phenomena modelled by the KPZ class include turbulent liquid crystals, crystal growth on a thin film, facet boundaries, bacteria colony growth, paper wetting, crack formation, and burning fronts [2].

The time derivative of the height function depends on three factors: smoothing (the Laplacian), rotationally invariant, slope dependent, growth speed (the square of the gradient), noise (spacetime white noise)

$$h_t(x,t) = \nu \nabla^2 h + \frac{\lambda}{2}(\nabla h)^2 + \eta(x,t)\tag{2}$$

where η is white Gaussian noise and ν and λ are non-zero parameters which can often be (heuristically) computed for a particular growth model directly from the microscopic dynamics.

(iii) One widespread example of the "Molecular Beam Epitaxy" (MBE) model, where material is slowly evaporated onto the surface at sufficiently high temperature. This deposition produces a film which bears an epitaxial relation to the substrate. The growth process of surface formations is regularized by surface diffusion. The evolution equation for the shape of the film surface can be written

$$h_t(x,t) = -K \nabla^4 h + \lambda_2 \nabla^2 (\nabla h)^2 + \eta(x,t),\tag{3}$$

where K and λ_2 are parameters. The smoothening term $-K\nabla^4 h$ expresses the surface diffusion. This expresses the evolution of a thin epitaxial film in the case when the film instability is caused by the epitaxial stress, the film surface energy is isotropic, and the film is thin enough so that wetting interactions between the film and the substrate are important.

(iv) The appearance of step instabilities can be described by the evolution equations. In the growth process two different types of instability may appear [21]. On of them is the step bunching when the density of steps does not keep constant. The steps prefer to gather in bunches separated by large terraces. Step bunching occurs while steps are straight, i.e., the dynamics can be described by 1+1 dimensional equations. In the presence of large desorption it can be modelled by

$$h_t(x,t) = -\nu\, h_{xx} + \gamma\, h_{xxx} - K\, h_{xxxx} + \lambda\,[h_x]^2\,, \qquad (4)$$

where γ and ν are parameters and $h = h(x,t)$ is the rescaled step shape in stepwise direction x. The term $-\nu h_{xx}$ is responsible for the instability, the second term expresses the surface energy and surface diffusion, the third nonlinear term is proportional of the coarsening dynamics at long time [24].

(v) The second type of instability, the step meandering when steps do not stay straight and start wandering. The dynamics of meandering depends on the asymmetry in the attachment. In the presence of strong evaporation the Kuramoto-Sivashinsky (KS) equation is used

$$h_t(x,t) = -\nu\, h_{xx} - K\, h_{xxxx} + \lambda\,[h_x]^2\,, \qquad (5)$$

which one is obtained from (4) with $\gamma = 0$. It is the typical equation of the spatio-temporal chaos. KS equation is derived for both electrochemical deposition (ECD) and chemical vapour deposition CVD.

(vi) In case of vanishing desorption and weak symmetry, the growth process and the rise of coarsening pattern are modelled by the conserved Kuramoto-Sivashinsky (CKS) equation.

$$h_t(x,t) = -\nu\, h_{xx} - K\, h_{xxxx} + \lambda_2\,[h_x]^2{}_{xx}\,. \qquad (6)$$

The term $-\nu h_{xx}$ is responsible for the instability, the nonlinear term $-\lambda_2\big[h_x^2\big]_{xx}$ is proportional to the flux. Experiments suggest that CKS describes the surface dynamics for MBE.

(vii) Anisotropic coarsening for the height fluctuations $h = h(x,y,t)$ is described
when the height deviates from the mean slope

$$h_t(x,t) = -h_{xxxx} - Ah_{xxx} - \left[h + h_{yy} + (h_y)^2 + Bh_x + Ch_{xx} \right]_{xx}, \qquad (7)$$

where A, B, C are parameters. The meandering instability is described by the
term $-h_{yy}$, the relaxation processes due to elastic step interactions are taken
into account with terms having an even number of x derivatives, the step
stiffness is incorporated in term $-h_{yyyy}$; the term proportional to A is related
to the dispersive nature of the step flow, the nonlinear term $-\left(h_y^2 \right)_{yy}$ is re-
sponsible for the coarsening.

The boundary conditions indicate the stress and the displacement continuity at the
film-substrate interface. The governing equation is considerably simplified if the
small-slope approximation is used, assuming that the slopes of the emerging sur-
face structures are small.

Numerical solutions to *Equations (1)–(7)* in 1+1 or 1+2 dimensions by means of
a pseudospectral method can be obtained with periodic boundary conditions. One
can observe the formation of hexagonal arrays of dots or pits in the parameter re-
gions predicted by the weakly nonlinear analysis. It is interesting that, similar to
the 1+1 case, the formation of two types of dots is possible: "cone"-like and "cap"-
like. With the increase of the supercriticality "cones" transform into "caps". It is
known that hexagonal patterns can become unstable with respect to patterns with
other symmetries

Results of the numerical simulations to *Equations (1)–(5)* show the transition
from hexagonal arrays of dots or pits to stripe patterns ("wires") with the increase
of the supercriticality. Transition from dots to wires in epitaxially strained films
has been observed in experiments [23].

The numerical solutions also show that quasiperiodic dodecagonal arrangement
of dots can be formed. However, this dodecagonal structure occurs only at the be-
ginning of pattern formation; later in time it either gets replaced by a hexagonal
structure, or grows further and ultimately blows up.

3. SURFACE ROUGHNESS

A common feature of most non-equilibrium interfaces is that their roughening fol-
lows simple scaling laws [5]. This phenomenon is also observed experimentally.
Here we define the mean height function $\bar{h}(t)$ at the time t for $t \in [0,T]$ by

$$\bar{h}(t) = \frac{1}{|\Omega|} \int_\Omega h \, dx \qquad (8)$$

where $|\Omega|$ is the area of $\Omega = [0,L]^2$. All rough surfaces exhibit perpendicular fluctuations which can be characterized by the surface roughness

$$w(t) = \sqrt{\frac{1}{|\Omega|} \int_{\Omega} \left| h(x,y,t) - \overline{h}(t) \right|^2 dx} \tag{9}$$

for $t \in [0,T]$.

In 1985, FAMILY and VICSEK [7] introduced the notion of "dynamic scaling" in order to incorporate both temporal and spatial scaling behaviors.19 Within this context, the evolution of the (saturated) rms width with deposition time t is characterized by a "growth" exponent β, according to σ is proportional to t^{β}. It is assumed here that the film thickness is directly proportional to the amount of material deposited and that the deposition rate is constant. The spatial and temporal scaling behaviours of films grown under non-equilibrium conditions can then be combined into the dynamic scaling form [1, 16]

$$w(L,t) = L^{\alpha} F\left(t / L^{\alpha/\beta} \right),$$

where $0 < \alpha < 1$ is referred to as the "roughness" exponent for the interface h and α/β is the dynamic exponent which describes the scaling of the relaxation time with system size L. The scaling function f has special properties, which indicates that $w(L)$ tends to a constant value L^{α} when $t/L^{\alpha/\beta} \to \infty$ and $w(L)$ is proportional to t^{β} when $t/L^{\alpha/\beta} \to 0$.

For the film growth, described by the KPZ equation, is associated with the exponents $\alpha = 0.385$ and $\beta = 0.240$, and for evolution described by (3) one gets $\alpha = \beta = 0$ [16].

4. NUMERICAL RESULTS

Using numerical simulations of the surface growth equation starting from a flat surface we can investigate the surface roughness w as a function of time t. The experimentally measurable layer thickness is $H(x,t) = Ft + h(x,t)$, where F denotes the mean deposition rate. In our calculation the amorphous thin film growth is represented by the one-dimensional deterministic field equation

$$h_t(t,x) = -h_{xx} - h_{xxxx} + (h_x)^2 - r(h_x)^2_{xx}, \tag{10}$$

which is a form of *Equation (4)* after rescaling. We note that r the parameters of the experimental setup, the details of kinetics and the deposition process are involved. The one-dimensional *Equation (10)* is solved with using Fourier spectral collocation in space and the fourth order Runge–Kutta exponential time differencing scheme for time discretization.

Gabriella Bognár

Applying the initial condition

$$h(0, x) = 0.01 \cos \frac{x}{16}\left(1 + \sin \frac{x}{16}\right)$$

to (10) the numerical solution for differently chosen r with parameters $x \in [0, 32\pi]$, $t \in [0, 250]$, $N = 256$, $\Delta t = 1/100$. The visualization of the cross section of the spatio-temporal evolution of the surface of the film calculated from the non-linear growth equation (10) are shown on *Figures 1–3* for time $t = 1000$ and for different values of parameter r.
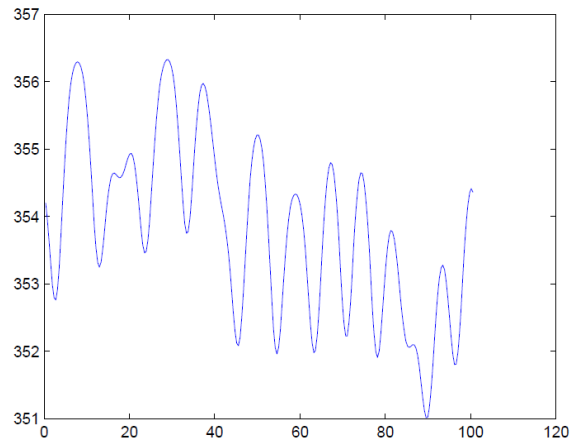
Figure 1. Height profile for $t = 1000$ and $r = 0.01$
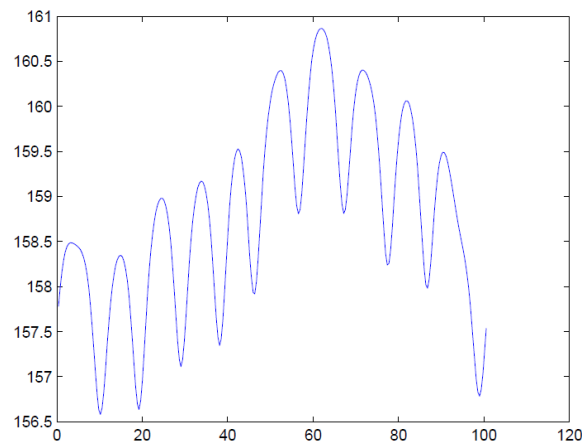
Figure 2. Height profile for $t = 1000$ and $r = 0.5$
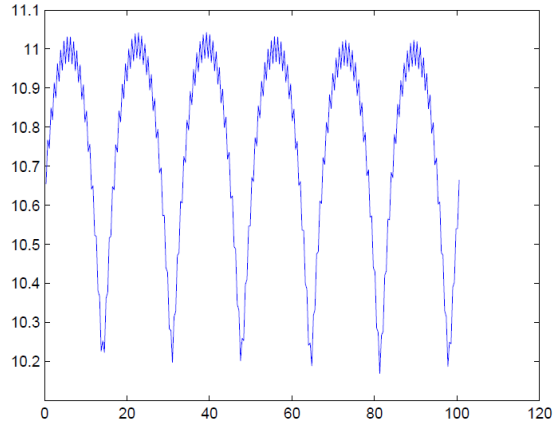
Figure 3. Height profile for $t = 1000$ and $r = 10$

The spatially average of the height profiles are exhibited with very similar figures in *Figure 4*.
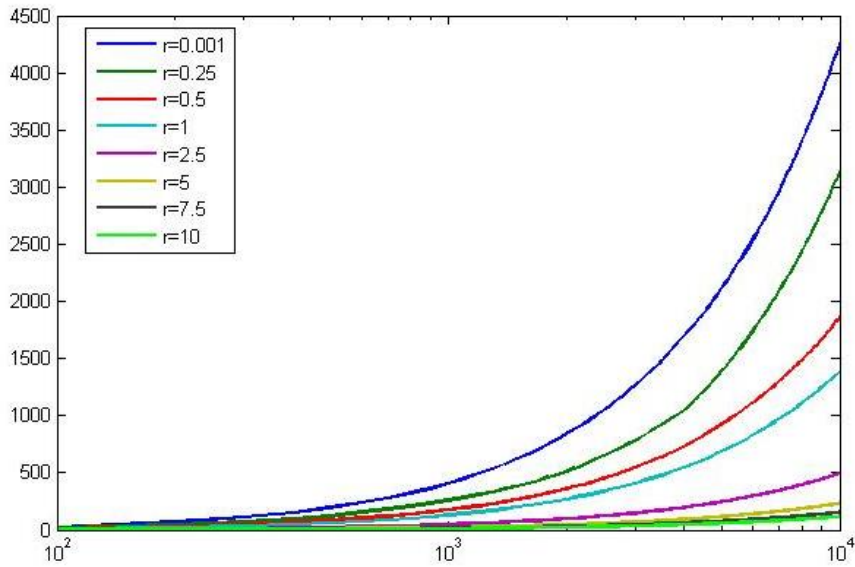
Figure 4. The average height profile $\bar{h}(t)$ for different values of r

The mean interface width $w(t)$ has been investigated for $r = 0.01, 0.5$ and 10, when

$$w^2(t) = \frac{1}{L} \int_0^L \left[h(x,t) - \bar{h}(t) \right]^2 dx .$$

These figures are represented on *Figures 5–7.*
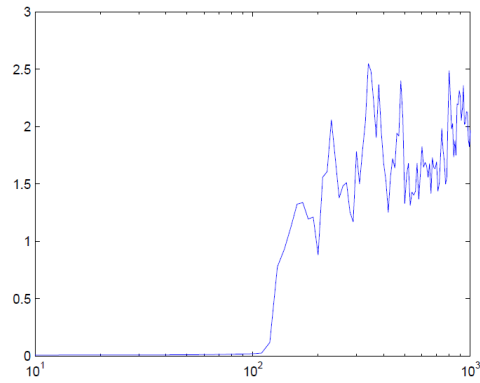
Figure 5. The profile of $w(t)$ *for* $t = 1000$ *and* $r = 0.01$
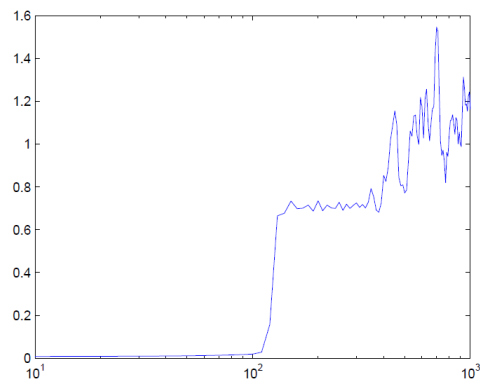
Figure 6. The profile of $w(t)$ *for* $t = 1000$ *and* $r = 0.5$
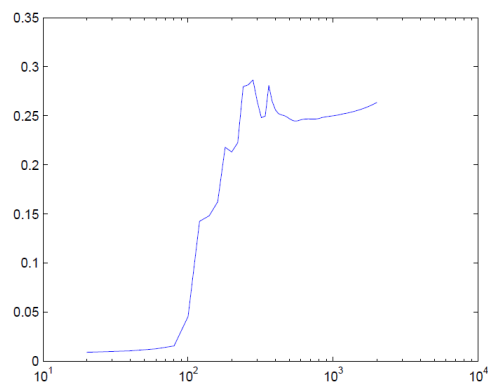
Figure 7. The profile of $w(t)$ *for* $t = 2000$ *and* $r = 10$

5. CONCLUSION

Based on the growth equation the better understanding of the amorphous thin film growth process is available. The temporal evolution of the surface roughness of the surface morphology with parameter data has been presented. The effect of the parameter is significant on the height profile, on the mean average height profile and the surface roughness. The spatio-temporal evolution of surface morphologies should be compared with experimental data for growth processes or sputter deposition.

REFERENCES

[1] BARABÁSI, A. L.–STANLEY, H. E.: *Fractal Concepts in Surface Growth.* Cambridge University Press, Cambridge, 1995.

[2] CORWIN, I: *The Kardar–Parisi–Zhang equation and universality class.* arXiv: 2011, 1106.1596v4.

[3] CROSS, M. C.–HOHENBERG, P. C.: Pattern formation outside of equilibrium. *Reviews of Modern Physics,* 65 (1993), 851–1112.

[4] CUERNO, R.–MUNOZ-GARCIA, J.–GAGO, R.–VAZQUEZ, L.: Universal non-equilibrium phenomena at submicrometric surfaces and interfaces. *Eur. Phys. J. Special Topics,* 146 (2007) 427–441.

[5] CUERNO, R.–BARABÁSI, A-L.: Dynamic scaling of ion-sputtered surfaces. *Phys. Rev. Lett,* 74 (1995), 4746.

[6] EDWARDS, S. F.–WILKINSON, D. R.: The surface statistics of a granular aggregate. *Proc. Roy. Soc. London,* Ser. A, 381 (1982), 17–31.

[7] FAMILY, F.–VICSEK, T.: *Dynamics of Fractal Surfaces.* World Scientific, Singapore, 1991.

[8] FEDER, J.: *Fractals.* Plenum Press, New York, 1988; BERRY, M. V.–LEWIS, Z. V. *Proc. R. Soc.*, 1980, A 370 459.

[9] FRISCH, T.–VERGA, A.: Effect of step stiffness and diffusion anisotropy on the meandering of a growing vicinal surface. *Physical Review Letters,* PRL 96 (2009), 166104.

[10] GILLET, F.–PIERRE-LUIS, O.–MISBAH, C.: *Non-linear evolution of step meander during growth of a vicinal surface with no desorption.* arXiv: cond-mat/0005422v1, 2000.

[11] GILLET, F.–CSAHÓK, Z.–MISBAH, C.: Continuum nonlinear surface evolution equation for conserved step-bunching dynamics. *Physical Review,* B 63 (2001), 241401(R).

[12] GOLOVIN, A. A.–DAVIS, S. H.–VORHEES, P. W.: Self-organization of quantum dots in epitaxially strained solid films. *Physical Review,* E 68 (2003), 056203.

[13] GOLOVIN, A. A.–NEPOMNYASHCHY, A. A.: *Self-assembly, pattern formation and growth phenomena in nano-systems.* Springer, Dordrecht, 2004.

[14] KARDAR, K.–PARISI, G.–ZHANG, Y. Z.: Dynamic scaling of growing interfaces. *Phys. Rev. Lett,* 56 (1986), 889–892.

[15] KHARCHENKO, D. O.–KHARCHENKO, V. O.–KOKHAN, S. V.: *Properties of nano-pattern formation in reaction-diffusion systems with hyperbolic transport and multiplicative noise.* arxiv: 1101.3189v1.

[16] KRIM, J.–PALASANTZAS, G.: Experimental observations of self-affine scaling and kinetic roughening at sub-micron length scales. *Int. J. of Modern Phys,* B 9 (1995), 599–632.

[17] KRUG, J.: Origins of scale invariance in growth processes. *Advances in Physics,* 46 (1997), 139–282.

[18] MUNOZ-GARCIA, J.–CUERNO, R.–CASTRO, M.: Short-range stationary patterns and long-range disorder in an evolution equation for one-dimensional interfaces. *Physical Review,* E 74 (2006), 050103(R).

[19] NAVEZ, M.–SELLA, C.–CHAPEROT, D.: *Etude de l'attaque du verre par bombardement ioniqué.* C. R. Acad. Sci., Paris, 1962, 254 240.

[20] PIERRE-LUIS, O.–DANKER, G.–CHANG, J.–KASSNER, K.–MISBAH, C.: Nonlinear dynamics of vicinal surfaces. *J. Crystal Growth,* 275 (2005), 56–64.

[21] POLITI, P.–VAIA, R.: *Steady states of the conserved Kuramoto-Sivashinsky equation.* arxiv: 0609545v1.

[22] RAMOS, S. M. M.–CHARLAIX, E.–BENYAGOUB, A.: Contact hysteresis on nano-structured surfaces. *Surface Science,* 540 (2003), 355–362.

[23] VALBUSA, U.–BORAGNO, C.–BUATIER DE MONGEOT, F.: Nanostructuring surfaces by ion sputtering. *J. Phys.: Condens. Matter,* 14 (2002), 8153–8175.

[24] VERGA, A. D.: Anisotropic dynamics of a vicinal surface under the meandering step instability. *Physical Review,* B 80 (2009), 174115.

INTEGRATED PRODUCT DEVELOPMENT BASED ON FORESEEING LIFE-CYCLE CONSEQUENCES

JONATHAN C. BORG

University of Malta, Department of Industrial & Manufacturing Engineering
Msida MSD 2080, Malta
jonathan.borg@um.edu.mt

Abstract: During product development, there is a *phenomena* that is continuously present, whether stakeholders are aware of it or not. This phenomena concerns the generation of Life-Cycle Consequences (LCCs) with design decision commitments. The understanding of this phenomena and how consequences are generated has been exploited to develop the 'Knowledge of Life Cycle Consequences' Approach. Evaluations performed via a number of computational prototypes based on this approach have repeatedly concluded that this approach allows designers to foresee consequences spanning multiple life phases. This approach thus promotes *Design Synthesis for Multi-X,* which is fundamentally different from an approach using multiple, standalone DFX methods. Thus the approach developed contributes a means of how to achieve integrated product development.

Keywords: Mechanical Design, DFX, Computer Aided Design, Product Development Metrics

1. INTRODUCTION

Industry is under increasing pressure to deliver products that cater for a host of total life-cycle requirements [1]. At the same time, the research reported in this paper highlights a neglected *phenomena* taking place during product development. A *phenomena* is similar to gravity: whether one knows about it, whether one is young or old, whether one understands how it operates, gravity is continuously acting upon us. Similarly, the *phenomena* addressed in this paper is continuously present during product development whether one is aware of it or not. This phenomena, called Life-Cycle Consequences (LCCs) is that 'Design phase decisions have consequences that propagate across different Product Life-Phases'.

Several cases of this phenomena have been documented by BORG [2]. Consider for instance the case when a designer *(Figure 1)* of say a thermoplastic part is during design synthesis, making the decision commitment to use a fastener such as a bolt, to assemble this part to a complex mechatronic system. The good intention of the designer was in this case to achieve easy dis-assembly (in the future servicing phase) unlike for instance using ultrasonic bonding. However, this commitment has a consequence that a hole of diameter ømm is required in this thermoplastic part. In addition, this commitment will now result in a consequence that the mould tool for mass producing the plastic part must requires a core pin, whose diameter must

take into consideration the hole diameter required as well as the shrinkage factor of the plastic to be used. The presence of the core pin will now give rise to a new consequence i.e. that weld line defects during will be potentially formed during the manufacturing phase. The weld line defects will in turn have a consequence on the part's structural integrity during the use phase that can result in more scrap.

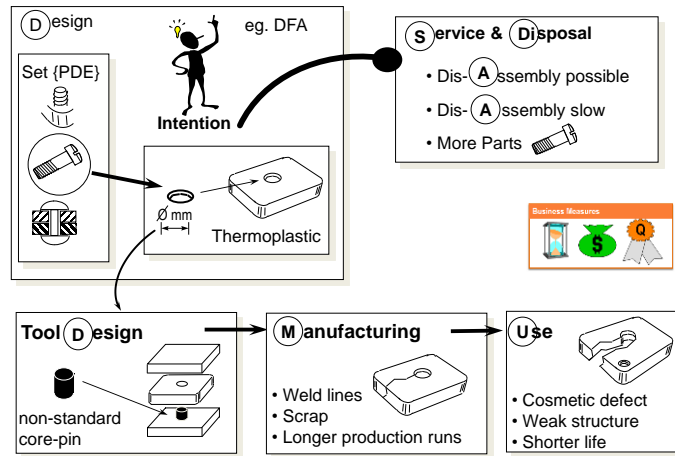*Figure 1. LCC phenomena: design decisions progagate across the whole life*

From case-study observations, a phenomena model [2] describing how life cycle consequences [LCC] are generated from synthesis decision commitments made under two different conditions has been generated, this schematically illustrated in *Figure 2*.
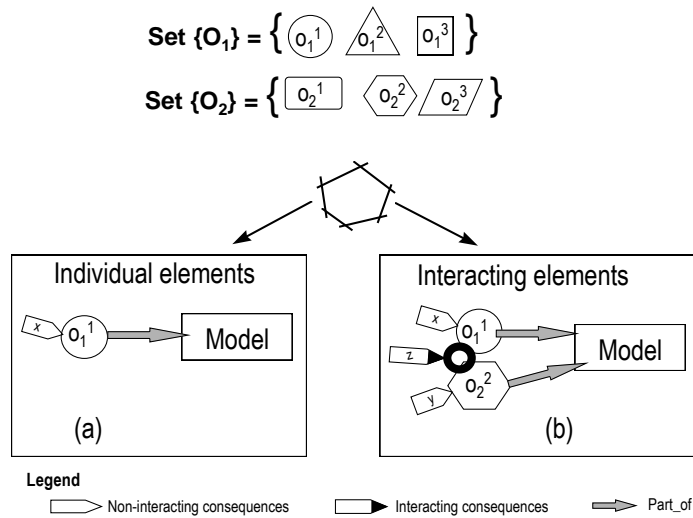

Figure 2. LCC phenomena model: interacting and non-interacting commitments

- **Non-Interacting LCC*ni***: Consequences in this case result during an arte-facts's life due to the presence of individual artefact design elements (e.g. a hole feature) or life-phase elements (e.g. a mould tool) introduced by synthesis decision commitments made independent of other synthesis elements present in the artefact life model.
- **Interacting LCC*i*:** Consequences in this case depend on a set of 'n' life synthesis commitments where n > 1.

These LCCs and the phenomena model established, indicate that there is a need of means by which LCCs can be foreseen and catered for. Otherwise, the consequences impacting the different life phases will negatively influence the performance of product development.

2. MEANS FOR HANDLING THIS 'LCC PHENOMENA'

A review by BORG and YAN [3] had established that approaches like team based [4], DFX [5][6], knowledge based [7], constraint based [8] and failure mode and effects analysis (FMEA) [9] are limited to supporting 'life-oriented' design synthesis so necessary for achieving integrated product development. Although team working brings all expertise together, it does not ensure that knowledge supporting design decision making is available continuously as team members are often working alone (see *Figure 3*), still making decisions in the interim period between design review meetings.
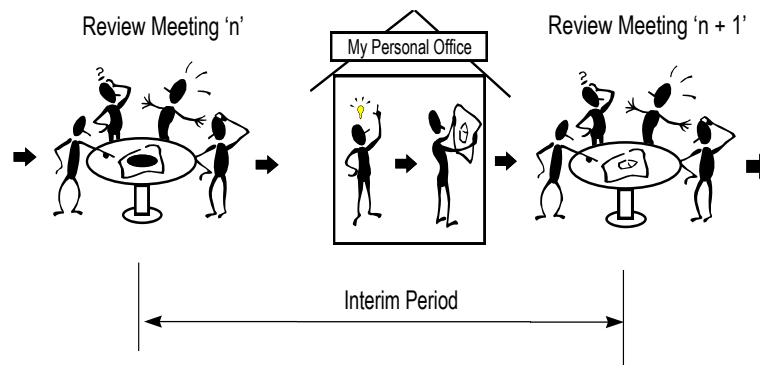
Figure 3. LCC: Decisions being taken in the interim period between team meetings

Thus, due to the phenomena of LCCs, interim period decision result in conseqeunces on the an artefact's life. Teams also have difficulties in recognizing the complex propagation effect of design decisions.

In "Design for X", a major drawback is that DFX knowledge tends to be segmented by artefact life-phase aspect (e.g. Design for Manufacture versus Design for Service). In addition DFX knowledge is employed late, for candidate solution analysis when major design decisions have already been committed. Further, DFX

knowledge is generic as it does not consider the actual resources that will be encountered by the artefact being design.

Knowledge-based (KB) design tools provide predictive modelling power with the breadth of life-phase expertise. However, this predictive power, is generally being employed for candidate solution analysis after design decisions committed. In addition, KB tools can only provide a narrow and segmented view of a candidate solution as knowledge captured tends to be of single life-phase view, making it difficult to explore trade-offs between multiple life-cycle aspects of an evolving design solution. A constraint network (CN) based approach requires a pre-defined network of parameter relationships describing the conceptual solution itself. This means that CNs provide support late in the design process. Further, their non-directional inference capability, whilst useful to supporting the cooperation between multiple perspectives, distorts the way designers work in reality because it results in a modelling world where there is no distinction between design characteristics that can be defined in reality by the designer and properties that are derived such as costs.

With *Failure Modes and Effects Analysis (FMEA)*, failure modes, mostly of the use phase, are identified late and subject to the analyst's design solution interpretation. Thus these different approaches exhibit one or more of the following limitations:

- they provide an insight into LCCs late in the design process;
- they provide a narrow and segmented insight into consequences being generated;
- they provide a generic insight rather than problem/company specific providence;

These limitations suggest that any *means* allowing designers, to have an early insight into LCCs influencing a number of life-phases, is highly desirable if Integrated Product Development is to be truly achieved.

3. A KNOWLEDGE OF LCCs APPROACH TO HANDLING PHENOMENA

Thus based on the identified phenomena of life cycle consequences (LCC) and the lack of available support means, this research embarked on developing a design approach concept aimed at exploiting relevant knowledge of LCC to help foster *Design Synthesis For Multi-X* which is core for truly achieving an Integrated Product Development Approach. The established phenomena model highlights that for generating a life-oriented design solution, *concurrent synthesis* of the 'artefact' and 'life-phase system' is a necessity if designers are to do 'Design Synthesis for Multi-X'. Otherwise, solution specific LCC_i will be difficult to reveal and cater for during synthesis. This understanding provides the basis to *what* should be captured and modelled to causally relate synthesis decision commitments and life cycle consequences. This understanding can therefore be exploited for:

- *foreseeing LCCs:* depending on commitments made, modelled LCCs co-evolving with the solution, can be revealed during synthesis to predict the influence on the measurements of life cycle performance;
- *solution synthesis guidance:* it provides a means to search for elements that need to be committed to result in an intended consequence; e.g. what PDEs result in a sub-assembly that is easy to dis-assemble in the disposal phase?
- *consequence avoidance/relaxation:* designers can be pro-actively made aware of consequences and their *source* commitments; this knowledge provides guidance to *what* specific commitments can be *explored* to avoid/relax a consequence revealed.

Using these foundations, the *'Knowledge of life-cycle Consequences (KC)'* approach framework to 'Design Synthesis for Multi-X' has been developed, based on the following three frames [2].

- *Operational frame:* this concerns the operating principles of the approach. Basically, it assumes that many well-developed solution concepts (PDEs) and well-known life cycle phase elements (LCPEs) are *re-used* during synthesis and encountered during the total life of an artefact. A fundamental operating principle of the approach is that a designer is engaged in concurrent synthesis – the *artefact life model* (consists of *artefact model* and *life-phase system models*) is *what* the designer generates during component life design synthesis. Essentially the approach supports a designer in making life-oriented synthesis decision commitments, by pro-actively and timely revealing LCCs co-evolving with a commitment. This awareness allows a designer to therefore foresee and take actions on artefact life-cycle consequences revealed. For this purpose, when a design sub-problem is encountered (step 1), the designer interacts (step 2) with a synthesis elements library to search for a set of suitable elements (step 3). Based on known *intentions, preferences* and *circumstances*, the designer commits (step 4) an element to evolve the artefact life model.
This evolving model is monitored (step 5) by *LCC inference knowledge* which reveals (step 6) any co-evolving LCCs. Relevant *LCC action knowledge* infers actions that need to be carried out, such as changes in performance measures of appropriate life-phase metrics to allow designers to monitor the artefact life behaviour. Collectively, this inferred knowledge is utilized by the designer (step 7) for exploring the avoidance/relaxation of the LCCs detected and for the handling of trade-off between conflicting LCCs associated with the evolving solution.
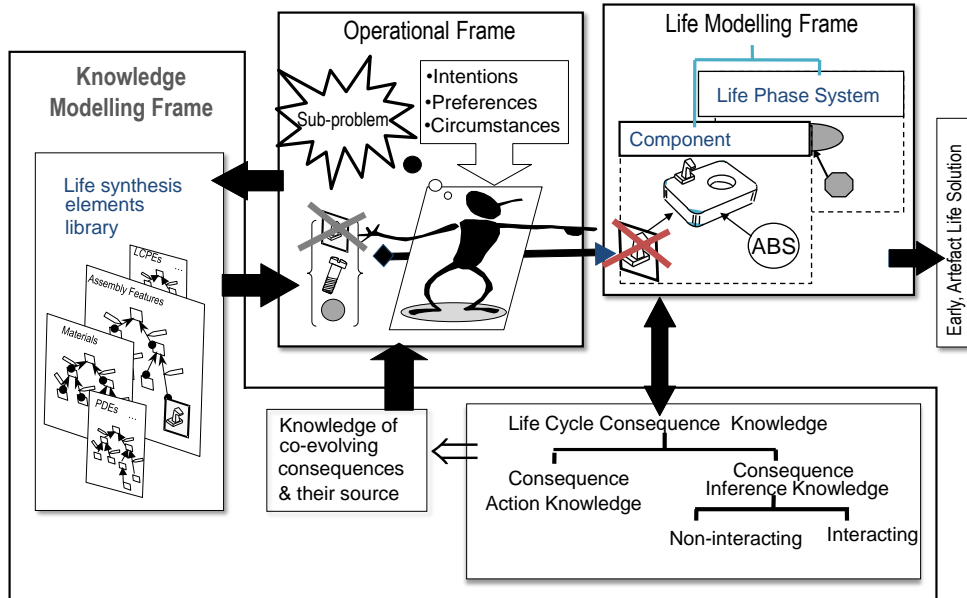
Figure 4. Established KC Approach Framework for handling LCCs

- *Artefact life modelling frame:* due to the need of concurrent synthesis, designers need to handle both artefact and life-phase system models. This frame therefore comprises a set of domain specific *synthesis elements* (PDEs and LCPEs) linked with *part_of relationships* describing the evolving compositional *artefact* and *life-phase system* models for a pre-set synthesis viewpoint, in this case from a constructional perspective;
- *Knowledge modelling frame:* This concerns the description of:
  - a synthesis element library, consisting of various models of synthesis elements (PDEs and LCPEs) reused within the design and life of a mechanical artefact domain. In the case of components, this includes models of form features, assembly features, and materials and LCPEs such as fabrication systems and assembly systems;
  - life-cycle consequence knowledge, consisting of:
    - LCC inference knowledge for revealing non-interacting and interacting LCCs co-evolving with synthesis decision commitments;
    - LCC action knowledge, for performing actions specific to a consequence inferred, this including LCC to performance mapping, concurrent synthesis patterns and guidance/explanation to LCC avoidance/relaxation.

4. EVALUATION OF THE 'KC' APPROACH FRAMEWORK

To evaluate the exploitation of the LCC phenomena model, the 'KC' approach framework has been implemented and adopted over the years in a number of prototype computational tools for a range of engineering applications including (i) thermo-

plastic parts [10] (ii) biomedical devices [11] (iii) collaborative design scenarios [12] (iv) intelligent sketching [13] (v) factory design [14] and (vi) emotional based product development [15].
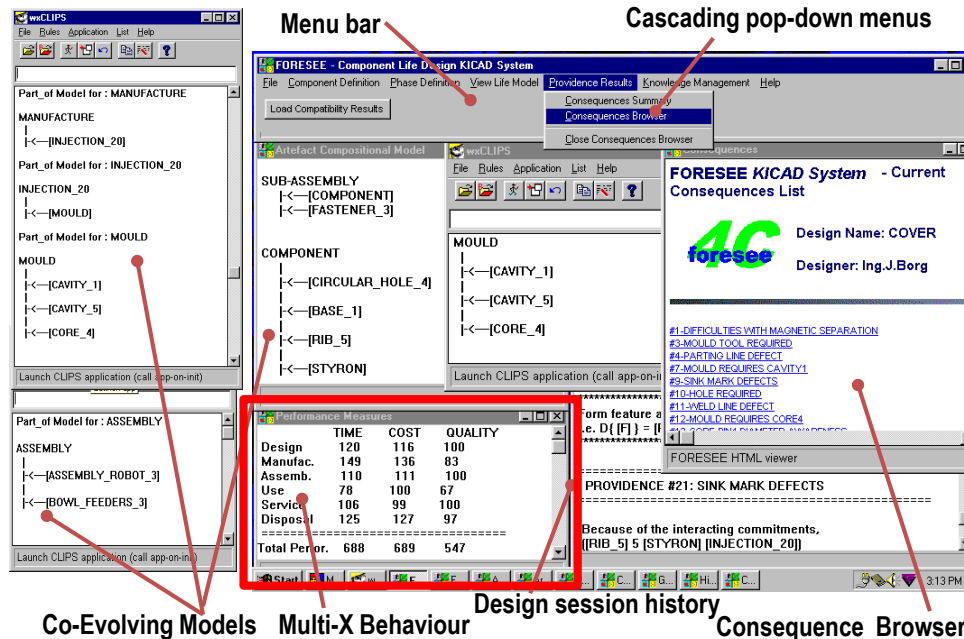
Figure 5. Screenshot of the FORESEE [2] Prototype System User Interface

For instance, the FORESEE system *(Figure 5)* developed for plastic part design was implemented as a Knowledge Intensive CAD (KICAD) employing a LCC knowledge model and implemented in a Windows environment using CLIPS [16]. For handling interacting commitments, FORESEE employed frame-based reasoning [17], this useful for modelling causality between interacting elements belonging to different abstraction levels in a *kind_of* taxonomy and life-cycle consequences. As illustrated in *Figure 5,* designers can see the impact of their decision commitments on a number of performance metrics in different life-phases via the *'Multi-X Behaviour'* window. In addition, designers can see the reasons for the generated LCCs as well as be guided on how to avoid/relax them through the *Consequence Browser.*

The various prototype implementations have established a number of strengths and weaknesses of the KC approach framework, namely that it:

- Proactively supports foreseeing of LCCs, across multiple phases, during solution synthesis and with least/specific commitments
- Raises awareness of consequences propagating across different life-phases helps influence the designer's thinking patterns;

- Motivates designers to 'explore' total life opportunities, avoid/relax detected LCCs;
- Assists in the conscious commitments of artefact life-phase system decisions;
- Supports the reuse of 'artefact life' scenarios;
- Integrates the activity of design synthesis with learning;
- however depends on the acquisition, addition and validation of a vast amount of LCC knowledge to be useful in practice;

5. CONCLUSION

The computational 'KC' approach framework presented in this paper *integrates* the activity of solution synthesis with the activity of foreseeing the artefact life behaviour. This integration makes the approach *fundamentally* different from *first generating* a solution and *later* analysing the candidate solution for conflicts with artefact life issues. It has been achieved by monitoring the fluctuation of various life-cycle performance measures. The positive evaluation of this approach through a number of different research projects at the University of Malta highlights that LCC knowledge plays a significant role in supporting designers to explore decisions' influences on multiple life-cycle metrics such as cost, tiem and quality. In addition, the author reports that the underlying phoneomena of LCCs has been very relevant in technical consultancy work performed for industry, as it helped untangle a number of mysterious causes to problematic issues faced during product development.

To concolude, capturing and codifying such LCC knowledge is therefore beneficial for developing intelligent digital design tools that proactively aid designers generate life-oriented design solutions. Thus, the *Knowledge of life-cycle Consequences* approach framework contributes a significant step towards the realization of $D_sF\Sigma X$ which is core to achieving *Integrated Product Development*.

REFERENCES

[1] ISHII, K.: Life-Cycle Engineering Design. *Transactions of the ASME,* 117 (1995), 42–47.

[2] BORG, J. C.: *Design Synthesis for Multi-X: a 'Life-Cycle Consequence knowledge' approach.* PhD Thesis. University of Strathclyde, UK, 1999.

[3] BORG, J.–YAN, X. T.: Design Decision Consequences: Key to ʻDesign for Multi-X' Support. *2nd International Symposium Tools and Methods for Concurrent Engineering.* Manchester, UK, 1998, 169–184.

[4] ASKIN, R. G.–SODHI, M.: Organization of Teams in Concurrent Engineering. In: DORF, R.–KUSIAK, A. (eds.): *Handbook of Design, Manufacturing and Automation.* New York, John Wiley & Sons Inc., New York, 1994, 85–105.

[5] MEERKAMM, H.: Design for X – A Core Area of Design Methodology. *Journal of Engineering Design,* Vol. 5, No. 2, (1994), 145–163.

[6] EASTMAN, C. M. (ed.): *Design for X: concurrent engineering imperatives.* Springer Science & Business Media, 2012.

[7] DIKKER, F.: *A Knowledge-based Approach to Evaluation of Norms in Engineering Design.* PhD. Twente, 1994.

[8] OH, J. S.–O'GRADY, P.–YOUNG, R. E.: A constraint network approach to design for assembly. *IIE Transactions,* 27 (1995), 72–80.

[9] NORELL, M.: The Use of DFA, FMEA AND QFD as tools for Concurrent Engineering in Product Development Processes. *International Conference on Engineering Design ICED '93.* Vol. 2. The Hague, 1993, 867–874.

[10] BORG, J. C.–YAN, X. T.–JUSTER, N. P.: Knowledge Intensive CAD of Thermoplastic Components. Research paper presented in the *IMTS2000 Manufacturing Conference* organized by the Society of Manufacturing Engineers (SME) held in Chicago, Illinois, USA, 2000.

[11] GRECH, A. K.–BORG, J. C.: Towards Knowledge Intensive Design Support for the Micro Surgical Domain. In: MARJANOVIC, D.–STORGA, M.– PAVKOVIC, N.–BOJCETIC, N. (eds.): *Proceedings of the Design 2008 10th International Design Conference.* Dubrovnik, Croatia, Vol. 1, 2008, 627–634.

[12] SPITERI, C. L.–BORG, J. C.: System architecture for mobile Knowledge Management within product life-cycle design. *International Journal of Manufacturing Research,* Vol. 5, No. 4 (2010), 396–412.

[13] FARRUGIA, P. J.–BALZAN, F.–BORG, J. C.: A Global Collaborative Design Framework for Sketch-Based Parametric CAD Modelling. *International Journal of Product Development,* Vol. 13, No. 1 (2011), 16–37.

[14] FRANCALANZA, E.–BORG, J.–CONSTANTINESCU, C.: Development and evaluation of a knowledge-based decision-making approach for designing changeable manufacturing systems. *CIRP Journal of Manufacturing Science and Technology,* 2016, doi: 10.1016/j.cirpj.2016.06.001.

[15] FARRUGIA, L.–BORG, J. C.: Design for X Based on Foreseeing Emotional Impact of Meetings with Evolving Products. *Journal of Integrated Design and Process Science,* Vol. 20, No. 2, 2016.

[16] GIARRATANO, J. C.–RILEY, G. D.: *Expert Systems: Principles and Programming.* USA, PWS, 1994.

[17] WALTERS, J. R.–NIELSEN, N. R.: *Crafting Knowledge Based Systems – Expert Systems Made Realistic.* New York, John Wiley & Sons, 1988.

CIRCULAR SAW BLADE VIBRATION ANALYSIS OF A RAIL CUTTING SINGLE-PURPOSE MACHINE

TAMÁS KUNDRÁT–ATTILA SZILÁGYI

University of Miskolc, Machine Tools and Mechatronics Department
3515 Miskolc-Egyetemváros
kundrattamas@gmail.com
szilagyi.attila@uni-miskolc.hu

Abstract: This article concerns the dynamical behaviour of a special circular saw blade operated by a rail-cutting machine. The dynamics, the eigenfrequencies and the stimulating frequencies are investigated, hence the vibrations of the circular saw blade of the machine is analysed. In this way we may draw some conclusions on the quality of the cutted surface. Since reworking has extra cost, precise cutting is expected already for the first trial. Vibrations coming from the cutting process may cause inaccurate manufacturing and, besides, may as well influence the lifetime of the saw-blade.

Keywords: rail cutting, saw blade, vibration, analytical and numerical analysis

1. INTRODUCTION

Rails are flexible support which made for running railway carriages and exposed to variable, heavy loads. Cutting rails is necessary clue to the following reasons. There are defined standards for the length of the rails; later segments are built in the fields with alominothermic welding. Besides we must use sidings at crossing tracks that allows turning from original way to another track. Using these ones, we have to join segments exceptionally accurately, because one may think that what would happened when a railway carriage with $50\frac{km}{h}$ would gone off the rails because of bad joints. Cutted surface quality is determined by dynamic behaviour and frequences of the saw blade, so eigenfrequences are important to keep prescribed quality.

2. CIRCULAR SAW BLADE FOR CUTTING RAILS

We have to use suitable tool for cutting which is able to cut the special Mn-alloyed steel and it has proportional cutting speed during processing due to the manufacturing time reduction. A saw blade material is expected to be carbide-tipped and relatively maintainable. HSS steel would be proper, although cutting speed can be increased by employing carbides. However these tools have high costs, we use them for cutting due to the productivity. The tool is a $\varnothing D = 630mm$

diameter segmental circular saw blade for this purpose by *GSP-High Tech Saws (Zborovice).*

2.1. Segmental circular saw blade

This tool composed of chrome-vanadium alloyed steel with hardened steel segments *(Figure 1)*. There are teeth on this segments which do the cutting. Segments are fixed with bolts to the steel body. The main advantage of this special saw blade is that it has short maintenance and repair time. It means, when the tool is damaged or it is overuse, replacing the segments with new ones we can use it further and continue cutting process. The number of the teeth is permanent in segments, although we have opportunity to expand application. The hardness of this tool is around $63-65$ HRC.
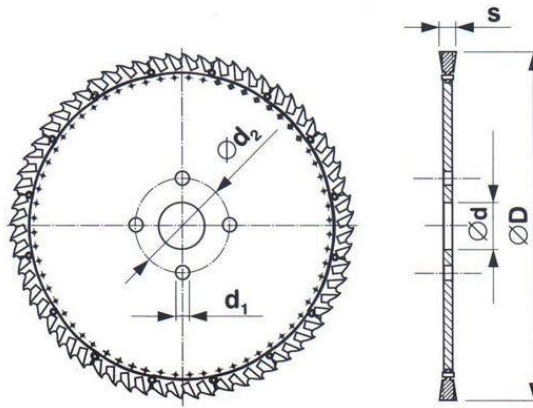
Figure 1. Segmental circular saw blade [1]

For the dynamic analysis and establishing the stimulating frequences, we apply the following details offered by the said company. $\varnothing D = 630mm$, $s = 6mm$, $\varnothing d_1 = 20mm$, $\varnothing d_2 = 160mm$.

3. ANALYTICAL VIBRATION ANALYSIS OF THE TOOL

First we create the saw blade dynamic model which is a circular disk. We constrained by its centerhole. We deal with such plane disk, whose thickness is much smaller the other two dimensions and it has permanent thickness, too.

3.1. The bending vibrations of a circular disk [2][3][4]

The general differential equation of plates in case of static load and small displacements is

$$\nabla^2\nabla^2\zeta = \frac{p}{D}, \tag{1}$$

where ζ is the transverse displacement of the disk, p is the external pressure, $D = \dfrac{E \cdot h^3}{12(1-v^2)}$ is the flexural stiffness and h is thickness of disk.

In *Equation (1)* differential operator means

$$\nabla^2\nabla^2\zeta = (\frac{\partial^2}{\partial x^2} + \frac{\partial^2}{\partial y^2})(\frac{\partial^2\zeta}{\partial x^2} + \frac{\partial^2\zeta}{\partial y^2}) = \frac{\partial^4\zeta}{\partial x^4} + 2\frac{\partial^4\zeta}{\partial x^2\partial y^2} + \frac{\partial^4\zeta}{\partial y^4} , \tag{2}$$

where x, y and z are the cartesian coordinates.

The part of inertial force on interface unit is

$$p_1 = -\rho h \frac{\partial^2\zeta}{\partial t^2} , \tag{3}$$

so disk's equation of motion takes the form of

$$\nabla^2\nabla^2\zeta + \frac{12\rho(1-v^2)}{Eh^2}\frac{\partial^2\zeta}{\partial t^2} = \frac{p}{D} . \tag{4}$$

During vibration the points of x, y coordinates on the surface of the disk perform displacement w at right angles to the disk plane. When $p = 0$, motion equation is

$$\nabla^2\nabla^2\zeta + \frac{12\rho(1-v^2)}{Eh^2}\frac{\partial^2\zeta}{\partial t^2} = 0 \tag{5}$$

and whose solution is

$$\zeta(x,y,t) = w(x,y)\cos\alpha t , \tag{6}$$

where α is angular frequency, t is time, x, y are displacement coordinates.

Differential equation of w amplitude function is

$$\nabla^2\nabla^2 w - \kappa^4 w = (\nabla^4 - \kappa^4)w = 0 , \tag{7}$$

where

$$\kappa^4 = \frac{\rho\alpha^2}{D} = \alpha^2\frac{12\rho(1-v^2)}{Eh^2} . \tag{8}$$

After the conversion of (6), the form of

$$(\nabla^2 - \kappa^2)(\nabla^2 + \kappa^2)w = 0 \tag{9}$$

is obtained, so the particular solutions of (9) can be reduced to the following simple differential equation's solutions

$$(\nabla^2 - \kappa^2)w = 0$$
$$(\nabla^2 + \kappa^2)w = 0$$
. \hfill (10)

Although there are infinite number of solutions of (7), we have to choose however those, which correspond to the current boundary conditions.

In the case of clamped parts the transverse displacements and rotation of the clamped surfaces satisfy conditions of (11)

$$w = 0$$
$$\frac{\partial w}{\partial r} = 0$$
, \hfill (11)

and on the unconstrained surfaces

$$\frac{\partial^2 w}{\partial r^2} + \nu \frac{\partial^2 w}{\partial s^2} = 0$$
$$\frac{\partial^3 w}{\partial r^3} + (2-\nu)\frac{\partial^3 w}{\partial r \partial s^2} = 0$$
, \hfill (12)

where r is the radial, s is the tangential coordinate.

In simple cases we can solve the above mentioned vibration equations exactly, however usually we have to use approximate solutions.

3.2. Circle plates vibrations [2], [3], [4]

To define vibration shapes and eigenfrequencies, the solutions of (7) needs to be set up in polar coordinate system. So the *Laplace operator*'s form in r, φ polar coordinate system is

$$\Delta = \nabla^2 = \frac{\partial^2}{\partial x^2} + \frac{\partial^2}{\partial y^2} = \frac{\partial^2}{r^2 \partial \varphi^2} + \frac{1}{r}\frac{\partial}{\partial r} + \frac{\partial^2}{\partial r^2},$$ \hfill (13)

then the vibration equation takes the form of

$$\left(\frac{\partial^2}{r^2 \partial \varphi^2} + \frac{1}{r}\frac{\partial}{\partial r} + \frac{\partial^2}{\partial r^2}\right)\left(\frac{\partial^2 w}{r^2 \partial \varphi^2} + \frac{1}{r}\frac{\partial w}{\partial r} + \frac{\partial^2 w}{\partial r^2}\right) - \kappa^4 w = 0 .$$ \hfill (14)

Solution of (14) is a vibration with n nodal diameter

$$w = f(r)\cos n\varphi .$$ \hfill (15)

Substituting (15) into (14), we get a normal fourth-order differential equation

$$\left[\frac{d^2}{dr^2} + \frac{1}{r}\frac{d}{dr} - \left(\frac{n^2}{r^2} - \kappa^2\right)\right]\left[\frac{d^2}{dr^2} + \frac{1}{r}\frac{d}{dr} - \left(\frac{n^2}{r^2} + \kappa^2\right)\right]f(r) = 0 .$$ \hfill (16)

The solution of (16) (which at a place $r = 0$ is not infinite) can be received from the following expression

$$f(r) = C_1 J_n(\kappa r) + C_2 J_n(\kappa r) \,, \tag{17}$$

where J_n is a first kind *Bessel-function* of order n and solutions can be specified depending on the boundary conditions. The C_1 and C_2 coefficients, depending on the boundary conditions, will give the shape modes during vibration. Due to the boundary conditions, a homogenous equation system for these coefficients is yielded. If this equation system's determinant is zero, we can get the frequency equation. In case of $n = 1$ the nodal diameter

$$\begin{vmatrix} J_0(\lambda) & Y_0(\lambda) & AI_0(\lambda) - BI_1(\lambda) & -K_0(\lambda) - \dfrac{2(1-\nu)}{\lambda} K_1(\lambda) \\[2mm] J_1(\lambda) & Y_1(\lambda) & I_1(\lambda) & -K_1(\lambda) \\[2mm] J_0(\alpha\lambda) & Y_0(\alpha\lambda) & I_0(\alpha\lambda) & K_0(\alpha\lambda) \\[2mm] J_1(\alpha\lambda) & Y_1(\alpha\lambda) & I_1(\alpha\lambda) & K_1(\alpha\lambda) \end{vmatrix} = 0 \,, \tag{18}$$

where $A = -1 + \dfrac{4(1-\nu)}{\lambda^2}$, $B = \dfrac{8(1-\nu)}{\lambda^3}$, J_n and Y_n are the Bessel functions of the first and second kinds, I_n and K_n are modified Bessel functions of the first and second kinds.

To analyse the circular saw blade we need some of the lowest eigenfrequencies, that can be defined on the basis of the roots of the homogenous equation system (18). To define solution we need previously described frequency parameter, which depends on disk's form, size and mode of supporting

$$\lambda^2 = \omega \cdot a^2 \cdot \sqrt{\frac{\rho \cdot h}{D}} \,. \tag{19}$$

where ω is circular frequency, a is the radius of the disk.

Knowing this, the following

$$f_{own} = \frac{\alpha}{2\pi} \tag{20}$$

relation between the angular and the natural frequencies can be defined

$$f_{nat} = \frac{\lambda^2}{2\pi \cdot a^2 \cdot \sqrt{\dfrac{\rho \cdot h}{D}}} = \frac{\lambda^2}{2\pi \cdot a^2 \cdot \sqrt{\dfrac{\rho h}{\dfrac{E \cdot h^3}{12(1-\nu^2)}}}} \,. \tag{21}$$

Based on [3] $\dfrac{b}{a} = \dfrac{40mm}{315mm} = 0,126984$ thus, in case of $n = 1$ nodal diameter, $\lambda^2 = 4$, as it can be approximated by simple calculations.

n	λ^2 for values of b/a of—							
	0.1	0.2	0.3	0.4	0.5	0.6	0.7	0.8
0	4. 235	5. 244	6. 739	7. 036	13. 05	20. 63	36. 60	81. 45
1	3. 482	4. 814	---------	9. 096	---------	20. 93	---------	45. 09
2	5. 499	6. 345	---------	10. 37	---------	21. 63	---------	67. 65

Figure 2. Frequency parameter values [3]

We consider some most often used vibration modes in practice *(Figure 3).* A detailed calculation for $n = 1$ case is performed in the followings.
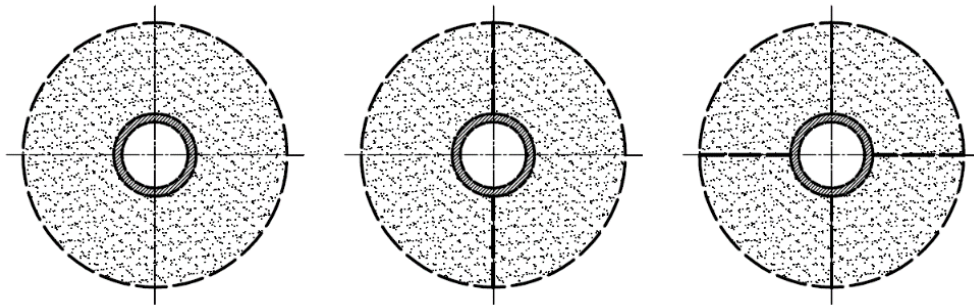

Figure 3. Permanent thickness plane disks vibration pictures [4]

3.3. Establishing one of the natural eigenfrequency of a circular saw blade – analytical method

In this chapter we define eigenfrequence of segmental circular saw blade with previously described method, which is used for analytical dynamic analysis. Based on the following consistencies

$$f_{nat} = \frac{\lambda^2}{2\pi \cdot a^2 \cdot \sqrt{\dfrac{\rho \cdot h}{D}}} = \frac{\lambda^2}{2\pi \cdot a^2 \cdot \sqrt{\dfrac{\rho h}{\dfrac{E \cdot h^3}{12(1-v^2)}}}} \tag{22}$$

$$f_{nat} = \frac{4}{2\pi \cdot (0,315m)^2 \cdot \sqrt{\dfrac{7827 \dfrac{kg}{m^3} \cdot (6 \cdot 10^{-3} m)}{\dfrac{199,948 \cdot 10^9 Pa \cdot (6 \cdot 10^{-3} m)^3}{12(1-0,27^2)}}}} = 58,333 Hz$$

3.4. The stimulating frequency of the tool

Due to the toolmaker company's brochure $v_c = 50 \dfrac{m}{min}$ is the optimal cutting speed for our circular saw blade. The rotational speed is

$$n = \frac{v_c}{r \cdot 2\pi} = \frac{50 \dfrac{m}{min}}{0,315m \cdot 2\pi} = 25,263 \frac{rotations}{min} , \tag{23}$$

The stimulating frequency while, as regards the number of the cutting teeth $z = 160$ is

$$f_{stimulating} = z \cdot \frac{n}{60} = 160 \cdot \frac{25,263 \dfrac{turn}{min}}{60} = 67,368Hz . \tag{24}$$

Resonance occurs when one of the eigenfrequencies of the saw blade and the stimulating frequency are equal or almost equal. In this case vibrations are formed in the tool and it is vibrating with relatively large amplitude. It may cause inaccuracy on cutted surface or may as well influence the lifetime of the saw blade.

3.5. The critical speed of the circular saw blade

Based on previously described calculations, it is clearly seen, that the danger of resonance is avoided employing by the suggested cutting speed, although the saw blade has a critical speed value, when the eigenfrequency and the stimulating frequency are equal. The

$$n' = \frac{60 \cdot f_{own}}{z} = \frac{60 \cdot 58,333Hz}{160} = 21,875 \frac{turn}{min} \tag{25}$$

$$v_c' = \frac{d \cdot \pi \cdot n'}{1000} = \frac{630mm \cdot \pi \cdot 21,875 \dfrac{turn}{min}}{1000} = 43,295 \frac{m}{min} \tag{26}$$

cutting speed is not allowed to be applied, since vibrations may be formed. During cutting process speed is much more smaller than the critical speed so we do not need to consider resonance, although at nearby the critical speed we also must not use the saw blade.

In this article we define eigenfrequency and critical speed for one vibrational mode; however there are endless vibration modes for each disc shape that we would have to analyse. Further, vibration modes have higher eigenfrequencies, so they differ largely from stimulating frequencies, so danger of resonance decreases. Although it may occurs the stimulating frequence is subharmonic of one higher eigenfrequence which also may causes resonance.

4. VIBRATION ANALYSIS OF THE TOOL WITH AN FEM (FINITE ELEMENT METHOD)

After some analytical results, in this section we are going to analyse the tool with a FEM software. Previously could be observed, when we clamp the saw blade on the middle of the disk, there is slight chance for the resonance at the specified cutting speed. As with the analytical method, we calculate both the natural and stimulate frequencies of the tool. Based on these values, we can be informed about the dynamic behaviour of the circular saw blade and the critical cutting speed of it.

We analyse three different cases with FEM. In first case like previous ones we use the model a disc clamped on the central hole. Diameter of the hole is $\varnothing d = 80mm$. Besides we also analyse a model which has 4 more holes with $\varnothing d_1 = 20mm$ on a $\varnothing d_2 = 160mm$ bolt circle. Due to these holes, dynamic stiffness of the tool is higher since the mass, which could be put into vibration decreases. Finally we analyse the case of the rotating disc. We expect the natural frequencies to increase, which would decrease the risk for the resonance. Although we can solve this case using analytical analysis, it is rather complicated, so we use FEA to solve this problem instead.

The density of disc material in case of steel is $\rho = 7827\frac{kg}{m^3}$, the Poisson's ratio is denoted by v with the value of $v = 0,27$. Young modulus is $E = 199,948GPa$.

4.1. First case – clamping the tool on the central hole
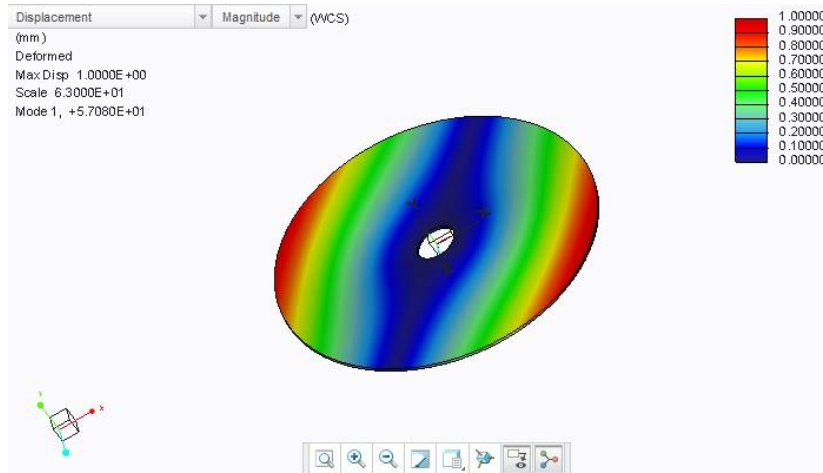

Figure 4. $\kappa = 1$ *shape mode of the saw blade – first case*

In *Figure 4* we can see displacements of the tool and mode 1 vibration picture. It means that there is $n = 1$ nodal diameter and $m = 0$ nodal circles. The lowest eigenfrequency is $57,080Hz$. Previously solved analytical analysis was successful, since eigenfrequency results are close to each other.

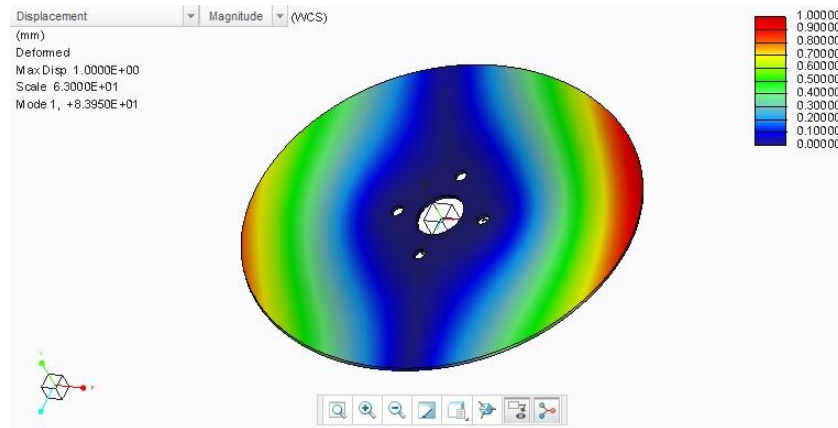## 4.2. Second case – clamping the tool on the central hole of disc and on more 4 holes along a bolt circle

Figure 5 Displacements of the saw blade – second case

In *Figure* 5 we also can see displacements of the tool and the lowest eigen-frequency. In this case it is $83,950 Hz$. It is also mode 1 vibration picture. Due to the 4 more bores, we obtained higher eigenfrequency, so the risk of the danger of resonance is sharply decreased. It means that cut surface is more precise because eigenfrequencies and stimulating frequency are far from each other.

4.3. Third case – clamping the tool like in case 2, but the rotation of the disc is considered

In this case the lowest eigenfrequency is $83,9502 Hz$. As the rotation of disk is low, centrifugal force will not influence the previously calculated eigenfrequency.

5. COMPARISON OF THE ANALYTICAL AND FEA RESULTS

In this article we created a model of circular saw blade and we did analytical analysis and FEA. We have calculated eigenfrequencies and the stimulating frequency. Based on them, we have considered geometries, the dynamical behaviour of the cutting tool and the danger of resonance. Due to the complexity, we solved only one case with analytical method. This case was when we clamped the saw blade by the central hole. This analysis seems to be successful, since eigenfrequency results are in correlation with those of the FEA. Eigenfrequency with analytical method was $58,333 Hz$ and with finite element method was $57,080 Hz$. We analyse more cases with FEM like holding tool with more 4 holes. The result was that eigenfrequency increased, since the tool has clamping higher dynamic stiffness. In the last case our analysis involved the rotating disc. The influence of the centrifugal force however, does not seem to be significated at such a low rotational speed.

6. SUMMARY

In this article was performed analytical and FEA analysis of a special circular saw blade of a rail cutting machine. We performed optimal tool for cutting rails and their features and we created approximately dynamic model for this. Based on vibration consistencies, the saw blade as a circular plate, we calculated the natural and the stimulating frequencies. We explored that vibration shape where resonance may occur most likely at suggested cutting speed. Finally we calculated that – for the smallest eigenfrequency – critical speed where vibrations with large amplitude would occur in the tool. In this case there may occur inaccuracy, form-and size problems on cutted surface. We should avoid this case all time.

ACKNOWLEDGEMENT

REFERENCES

[1]   https://katalog.mav.cz/detail.php?id=69742

[2]   PONOMARJOV, Sz. D.: *Static countings in engineering.* Vol. 6. Technical Publisher, 1966.

[3]   LEISSA, Arthur W.: *Vibration of Plates, NASA SP-160.* Washington, D. C., 1969.

[4]   LUDVIG, Győző: *Dynamics of machines.* Technical Publisher, Budapest, 1973, 537–540.

AUTOMATION OPTIONS OF SINGLE-PURPOSE MACHINES

GERGŐ LESKÓ[1]–GYÖRGY TAKÁCS[2]

[1]Bsc student, lesko.gergo@outlook.hu
[2]associate professor, takacs.gyorgy@uni-miskolc.hu
University of Miskolc, Szerszámgépészeti és Mechatronikai Intézet
Machine Tools Department
3515 Miskolc-Egyetemváros

Abstract: The basic aim of this paper is to discuss the automation opportunities, difficulties, problems and possible solutions of the designing of single-purpose machines, which are widely applied. Another aim is to use the computer optimally when designing these types of machines and to reduce the time of the designing as much as it is possible.

Keywords: Single-purpose machine, designing, optimization, function contraction

1. INTRODUCTION

In our speeded up world in the competition sphere, where we have to react to the demands of the market very quickly, it is indispensable to manage with the time. The company that replies the quickest to the market demands, can stay in competition. The earlier the reply arrives with the tender, the bigger the chance for the company to win a project. Before the company makes decisions they make financial calculations. In case of components required in smaller or bigger amount, it is necessary to decide, which type of machine worth more. There can be a lot of solutions but basically two of them are possible. One of them is to build a single-purpose machine to a certain problem or occupying CNC machines. There are less and less single-purpose machines used in production, because nowadays the application of CNC machines is advantageous even if there are small amount of workpieces. As well as due to the fact that the CNC machines are universal, they can be applied in the production of other components, too. But in case of single-purpose machines it is not true. There can be significant financial differences between the mentioned opportunities. Due to this, the leaders of the companies have to take a huge risk when they organise a project. It can result more difficulties that there is not enough time to think the decisions over. The prices of CNC machines are given, but in case of single-purpose machines we have to build the machines around the workpiece. The prices of single-purpose machines depend on the planning and the construction, so we have to plan the machine with good approximation to value the expected cost. Therefore more and more companies deal with automation options of single-purpose machines [1], [2].

In the following we will introduce an algorithm, which helps to make the designing some periods of single-purpose machines automatic so golden hours can be spared for companies.

2. PLANNING OF SINGLE-PURPOSE MACHINE

We can see the planning steps of single-purpose machines in *Figure 1*.
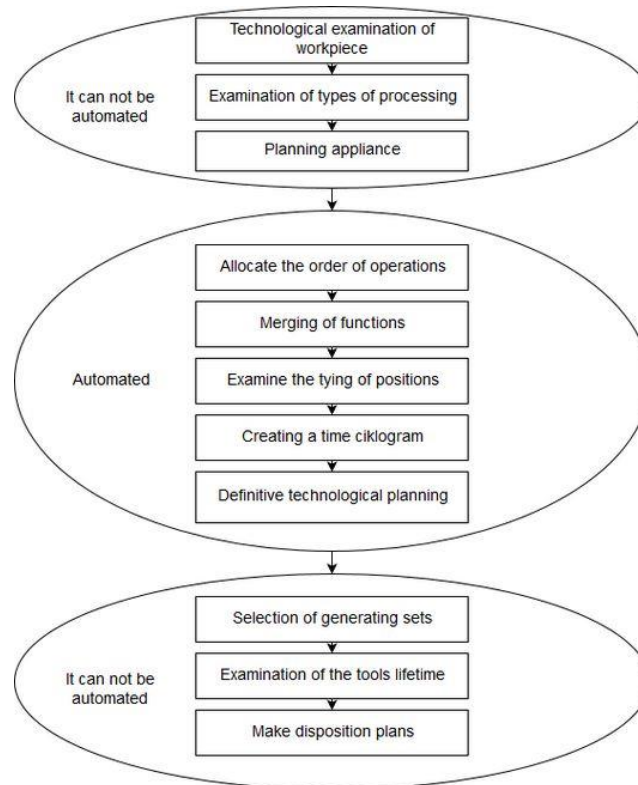

Figure 1. Planning steps of single-purpose machines

First and basic operation is to analyse the piece. Since we have to build the machines around the piece, we have to examine the attack directions that are needed to process and after that we have to decide where we can clamp the workpiece. It is important to examine what kind of processing is needed and what type of technology have to be used to finish machining and of course we also have to examine that we can keep the prescribed tolerance. The next step of the designing is merging of functions. Since the basic aim of single-purpose machine is to create a component as soon as possible, it is important to do serialization and collimation during the processing. The concentration regime of operational tools helps us. Based on this we distinguish first degree, second degree and third degree concentration [3]. Next we will show the characteristics of these concentrations.

2.1. Merging of functions

I: First degree spatial merging

The aim of first degree spatial merging is to merge tools -which take effect from the same attack directions- to common axis of rotation. The result is the complex tool.
Conditions:
1. The order of finishing each surface cannot be changed as the result of the merging.
2. Technology compatibility: The revolution of tool edges, which are on the same axis of rotation are the same but the distance of the axis can change, and in this way there are different cutting speeds. The feeding speeds are the same too so we have to synchronise them.
3. By complex tools it is necessary to pay attention to chip removal, cooling, strength, the accurate settings of the edges and exchangeability.

II. Second degree spatial merging

The aim of second degree spatial merging is to merge tools, group of tools -which take effect from the same attack directions- to common feeding unit. The result is the multi-spindle gear.
Conditions:
1. The order of finishing each surface cannot be changed as the result of the merging.
2. If the tools are on common gear they have the same feeding speed. Feeding speeds have to be synchronized. The revolution of the tool is n_i, the feed is f_i, so the feeding speed is $v_{ei} = n_i \cdot f_i$. It will work if the feeding speed of every tool is the same.
3. Both the rotational speed and the direction of rotation can be different.
4. It is not possible to merge the tools of surfaces which are in different processing phase within one gear.
5. Geometric compatibility: Tools – which are mounted in gear – have to fit. Distances of the axes have to be as big, that the bearings of the suitable strength spindles could fit. As well as, the necessary cutting performances have to be given to each tool.

III. Third degree spatial merging

The aim of third degree spatial merging is to group operational tools around the workpiece and to shape common working space. Results of this merging are the positions of single-purpose machines and the version of positions. According to the merging the structure sketch of single-purpose machines can be realized and after that we can decide what kind of aggregate units have to use to build a single-purpose machine.

Conditions:

1. The order of finishing each surface cannot be changed as the result of the merging, but if there is not any technological limit it can be interchangeable the chronology of group tools which take effect from the same attack directions.
2. Do not disturb technologies in common working space and position!
3. There should not be significant differences among cutting performances otherwise there will be large differences among forces.
4. The processing units need enough place in positions in order to be carried out the changing of tools, the cleaning and the task of maintenance.
5. The single-purpose machine has to be repairable.

According to these geometric and machining theory consideration and of course the concentration regime of operational tools we can automate the merging of functions all we need is an universal code system – which expands every parameters of the workpiece – from the workpiece. Thereinafter we will examine the merging of functions from the viewpoint of bores.

2.2. Difficulties of function merging from the viewpoint of bores

The first problem is come from that the computer's algorithm has to recognise the bores on the technical drawing. Furthermore it has to decide, which way will be the best to drill a bore, from below or from above, how to merge more surfaces to processing or how will be enough place to the unit of processing. It has to recognise the axis of bores, that these axis are coincident or not, or axis have an intersection or not. If the axes are coincident, it has to be examined – knowing diameters – that which bore we have to start the processing with. If the axis has intersection in one plane, it has to take cognizance the depth of bore and it is allow the collimation or not. In case of the axis are skew it has to examine the depth and the diameter of bores and certainly examine that there are enough material between the bores. In case of processing more bores it has to make an order among the processing and it has to recognise which flow will be the next. If it is not working the tools can be broken. Because of the easier transparency we have to perform these requirements that the user will not have to give too much data.

Computers need codes and mathematical operations but the users need easy manoeuvrability, minimal energy input and of course easy-to-learn code system. Thereinafter there will be a proposal which satisfies these requirements.

3. OPERATION OF BORE RECOGNITION ALGORITHM

If there is not a model in 3D, the computer has not enough information to recognize the bores of the workpiece automatically. That is why we have to supply the bores with codes which have got enough information content for computer processing. Every type of processing [4] which can be perceived by technologist we have to

supply by a letter during the encoding. This letter will be referred to the nature of processing.

Letters of processing:
 1. D: broaching,
 2. E: chamfer,
 3. F: drilling,
 4. FB: enlargement of bore,
 5. H: front countersink,
 6. M: threading,
 7. S: countersink.

Of course, during the processing the order is important, for example we cannot do broaching or threading while there is not any bore.

The order of precedence among the flows:
 1. Drilling (F) if it suits the diameter requirements it can be merged with chamfer (E) and front countersink (H).
 2. Enlargement of bore (FB), chamfer (E), and front countersink (H).
 3. Countersink (S).
 4. Broaching (D).
 5. Threading (M).

Processing from the same level can be parallelised if there are not any geometric limits or conflicts.

Since we talk about bores and bore type of processing we have to define cylinders in the space. To this we have to use a universal coordinate system. This coordinate system can be taken every point by user, but the suggestion is assign the XY plane to the sectional images, assign the XZ plane to plan view and assign the YZ plane to the side view, as you can see in *Figure 2*. This kind of coordinate system definition can be used for all of the workpieces.

After that we can define spatial cylinders. According to [5] for defining a cylinder we need the centre of the cylinder (point C), need the direction vector of the cylinder axis (vector $\vec{w}$), furthermore need the r radius and the h height *(Figure 3)*.

According to these we can give all points of the cylinders with the next formula:

$$P(\theta, t) = C + (s \cdot \cos \theta) \cdot \vec{e_x} + (s \cdot \sin \theta) \cdot \vec{e_y} + t \cdot \vec{e_z}. \qquad (1)$$

Where $0 \leq s \leq r$; $\qquad |t| \leq \frac{h}{2}$; $\qquad \theta \in [0, 2\pi]$.

To the operation of algorithm we not need to give the centre of the cylinders just the starting point of the bores, after that the program by means of a constant multiplier changes the starting point of the bores to the centre point of the bores. Here is the constant multiplier:

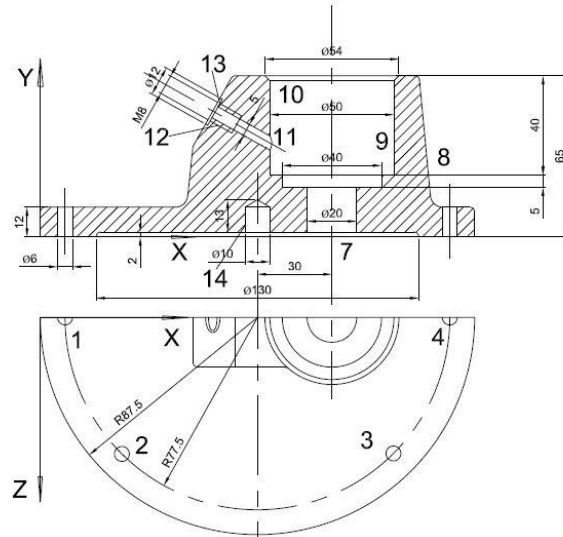$$Const = \frac{h}{2} \cdot |\vec{w}|. \qquad (2)$$
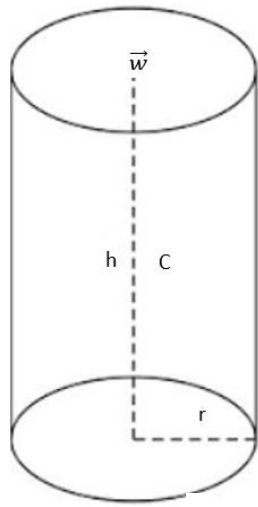
Figure 2. Defining coordinate system

Figure 3. Remarkable points and lines of a cylinder

To give the direction vectors of the cylinders can be difficult. The first angle that we mark with θ is in XY plane. This angle is between the axis of bore in XY plane and the X axis. The other angle that we mark with γ is between the axis of bore and the XY plane. In *Figure 4* we can see how to take the angles.
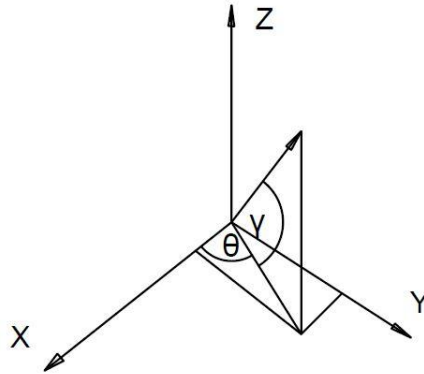
Figure 4. Define the axis of cylinder

The direction vector of the bore axis can be given with these angles. Here is the formula:

$$\vec{w}=(\cos\theta \cdot \vec{e}_x + \sin\theta \cdot \vec{e}_y) \cdot \cos\gamma + \sin\gamma \cdot \vec{e}_z. \tag{3}$$

So here is the code that the user should give in case of bore by the user:

$$A(F;C(x,y,z);\theta,\gamma;r;h). \tag{4}$$

The examination of cylinders (in this case bores) will start when we give two or more codes of bores to the program. The algorithm is the next in case of group of bores. First of all we have to count a vector $\vec{D}$, which is the difference of the centre points of the two cylinders:

$$\vec{D} = C_1 - C_0. \tag{5}$$

After that we take the two direction vectors of the cylinders and make a vector multiplication. The result is a vector which is perpendicular to the two direction vectors of the cylinders. This vector will be important later because with the help of it the program will foist planes and examine if the cylinders cut each other, or not:

$$\vec{M} = \vec{w_0}\times\vec{w_1}. \tag{6}$$

Then we calculate the length of these vectors.

The main reason why we have to calculate the length of the vectors will be clear with understanding the next formula (7):

$$|\vec{a}\times\vec{b}|=|\vec{a}| \cdot |\vec{b}| \cdot \sin\alpha. \tag{7}$$

A multiplication is zero when one of their factor is zero. The two vector cannot be zero, because these are the direction vectors of the cylinders, so just the $\sin\alpha$ can

be zero. If the $\sin \alpha$ is zero the axis of cylinders are parallel. If it suits the requirements of diameter, the bores – and with the bores, processing too – can be merged. In other case the axis of cylinders are not parallel so other type of test is needed. In case of parallel there are two possibilities: firstly we have to examine the distance of the two bores. We have to add the radius of cylinders after that we have to subtract the centre distance of cylinders from the sum of radii. On the other hand the cylinders can cut each other because of the height. If there are not parallel we have to run a five-step test. These tests generate planes between the cylinders. If these planes cut the cylinders, the processing cannot be merged.

In case of merging bores, there is not enough to compliance to the geometric requirements. Thereinafter we will examine the bores from the viewpoint of machining theory.

We have to expand the main code with three new parameters. These parameters high percentage of it are given by manufacturers beside to their products. The three new parameters are cutting speed *(v_c)*, feedrate *(v_f)* and the feeding force *(F_f)*. Here is the general shape of code which is expanded by these three parameters:

$$A(F;C(x,y,z);\theta, \gamma;r;h;v_c,v_f,F_f). \tag{8}$$

Conditions of technological compatibility in case of bores in one axis:
1. The maximum diameter of bores is 15 mm, the bore is bigger than this have to be drilled a much smaller-sized tool [4].
2. The difference from the optimal cutting speed cannot exceed ±21,5% in case of bores along one axis [4].
3. The lifetime of the tools have to be the same or multiple of each other.
4. The main drilling machine time have to be multiple of each other.

On the basis of consideration which is described above, we can see the encoding of the workpiece shown in *Figure 2*.

```
 1 F,20,12,0,–90,0,6,12,330,3.5,300
 2 F,97.5,12,134,–90,0,6,12,330,3.5,300
 3 F,252.5,12,134,–90,0,6,12,330,3.5,300
 4 F,330,12,0,–90,0,6,12,330,3.5,300
 5 F,252.5,12,–134,–90,0,6,12,330,3.5,300
 6 F,97.5,12,–134,–90,0,6,12,330,3.5,300
 7 F,205,17,0,–90,0,10,17,416,6.1,450
 8 F,205,22,0,–90,0,20,5,416,5.3,900
 9 F,205,60,0,–90,0,25,40,416,4.7,1100
10 E,205,62,0,–90,0,27,2,416,4.41,1150
11 F,145,55,0,–30,0,2.5,15,416,7.4,250
12 M,145,55,0,–30,0,4,10,130,4.8,100
13 H,145,55,0,–30,0,6,15,416,6.2,300
14 F,175,0,0,90,0,5,13,416,6.1,300
```

4. SUMMARY

According to the geometric and cutting theories detailed and defined above, the computer can make a sequence plan and it can specify the numbers of serial or parallel processing in case of bores. The principle and the realisation can reduce the time of planning largely by missing or jumping some steps. Thereinafter this principle will be extended to the milling featured processing too. Furthermore, the end goal is that the computer would be able to offer the user a sequence of operations and optimal structures of single-purpose machines. It will help companies to save time during the planning phase.

ACKNOWLEDGEMENT

REFERENCES

[1] SWANT, R.–BARAWADE, R. A.: *Design and development of spm a case study in multi drilling and tapping machine.*

[2] TOLOUEI-RAD, Majid: *Intelligent Analysis of Utilization of Special Purpose Machines for drilling Operations.*

[3] TAKÁCS, Gy.–ZSIGA, Z.–SZABÓNÉ MAKÓ, I.–HEGEDŰS, Gy.: *Gyártóeszközök módszeres tervezése.* Nemzeti Tankönyvkiadó, 2011.

[4] *Manufacturing Technology II.* http://fmcet.in/MECH/ME6402_uw.pdf (letöltés ideje: 2016. 06. 02.)

[5] http://www.geometrictools.com/Documentation/IntersectionOfCylinders.pdf (letöltés ideje: 2016. 03. 24.)

[6] ERDÉLYI, F.(ed.): *Szerszámgépek automatizálása II.* Miskolc, 1985.

VIBRATION ANALYSIS OF A MANUFACTURING DEVICE

ATTILA SZILÁGYI–GYÖRGY TAKÁCS–DÁNIEL KISS–
DÁNIEL TÓTH

University of Miskolc, Department of Machine Tools
3515 Miskolc-Egyetemváros
szilagyi.attila@uni-miskolc.hu takacs.gyorgy@uni-miskolc.hu;
kiss.daniel@uni-miskolc.hu; toth.daniel@uni-miskolc.hu

Abstract: This article introduces the instrumental vibration analysis of a large-sized manufacturing device for face-milling rectangular aluminium ingots. Firstly, potential vibration sources of the machine and its environment were counted and their frequency territory and characteristic frequency values were assessed. With the help of the appropriately placed vibration sensors, oscillations from different conditions of the equipment were sampled, on the score of generated spectrums, the assumed vibration sources were tried to identify, furthermore their ponderosity in spectrum and exerted influences on machine were estimated.

Keywords: vibration sources, measuring instruments, exciting frequencies

1. INTRODUCTION

The instrumental vibration analysis of a large-sized face-milling device is detailed in this article. This machine is applied for the improvement of the surface quality of aluminium ingots manufactured by face-milling. This operation is required by the high demands made on the multi-layered rolled aluminium products from the side of the automotive industry. The remanent surface roughness however, as the result of the face-milling process, often brings forth problems in the forms of bubbles, inclusions during the subsequent multi-layered rolling procedure. To eliminate this problem, several technological experiments, investigations and modifications had been carried out and implemented, the surface roughness of the ingots, however, still have not been approved enough, and not always met the requirements. In summary, some 50% improvement of the surface quality had been achieved as the result of the technological investigations [1–3]. Besides these improvements, which still have turned out to be unsatisfactory in several cases, investigations have revealed additional concerns. The theoretical surface roughness for example, which comes purely from the geometry of the cutting inserts, the feed rate and the depth of cut, still has not been able to be achieved, hence some other sources of the surface errors need to be searched for, which might come from the dynamic properties of the manufacturing device. These vibration sources are to be revealed by both experimental and theoretical means. This paper is to give some overview on the steps carried out during the experimental investigations.

2. THE GOAL AND THE METHOD OF ANALYSIS

The main objective of the instrumental vibration analysis is the exploration of those vibration sources, which influence the face-milling operations and occur in the device or its environment, just as the introduction and estimation of the induced oscillations' effects to the surface waviness. Thereunto by the help of appropriately chosen and placed vibration sensor and beside of properly adjusted sign-conditioning parameters, the evolving vibration samples will be recorded, then with the means of secondary signal processing (the spectrum-analysis of recorded samples), the previously considered vibration-sources and their weigh in spectrum are identified and from these factors, the exerted influences on the surface quality were inferred.

3. THE POTENTIAL VIBRATION SOURCES

In the factory – due to activities carried out there – several vibration sources are present, independent from the milling-device, of which the oscillation – propagating partly in the ground, partly through the air – can get into the workspace of the equipment. Such sources, but not limited to them, might come from the bridge crane passing over the equipment from time to time, the fork-lift carrying heavy weight rolled plate products, the high voltage electric induction of heating furnaces, the raw aluminium ingots hitting the ground following transport, the vibrations of other machines' auxiliary equipment (pumps, fans, hydraulic units) located in the factory. These sources summary are called the environmental sources, and their synergies are considered. During registering the environmental vibrations, the milling-device is at resting condition and off.

Derived from ingot-milling instrument, deemed more relevant excitations may be:

- imbalanced rotary weights,
- eccentrically rotary weights,
- driven (deformed) shafts,
- uniaxial error,
- different errors of the gear drive,
- mechanical clearances, gaps related errors,
- errors derived from cutting process.

Identifying of the vibration sources listed above is accomplished by the spectrum-analysis of vibration diagrams adopted from sensors. The necessary vibration diagrams are recorded in idle and during cutting process too. As there are three rotary units operating at constant rotational speed within the instrument (2 pieces of motor-shaft and the milling tool-spindle unit), thus frequencies of the certain vibration sources – in the course of spectrum-analysis – were correlated to either of these two different rpms, as basic frequencies.

The rotational frequency of electro-motors is $f_m = n_m/60$, the spindle is $f_o = n_o/60$, where $n_m = 1500$ [min^{-1}] and $n_o = 530$ [min^{-1}] are the rotational speed of

motors and spindle. Based on these, $f_m = 25\ [Hz]$ and $f_o \approx 9\ [Hz]$ are yielded to the rotational frequency. L_{f_m} and L_{f_o} indicate the level values for the rotational frequencies. The *Table 1* below contains the typical frequency-rates and levels of the milling-device's vibration sources.

Table 1
Considered relevant vibration sources of the ingot milling machine [4] [5]

Vibration-source	Occurrence	Characteristic frequencies [Hz]
Unbalanced rotary weights	Inductors of electro motors	$1 * f_m$
	Shafts of the input gears	$1 * f_m$
	Spindle + milling disk	$1 * f_o$
Eccentrically rotary parts	Inductors of electro motors	$1 * f_m$
	Shafts of the input gears	$1 * f_m$
	Spindle + milling disk	$1 * f_o$
Bended, deformed shafts	Shafts of the input gears	$1 * f_m, 2 * f_m$, where $L_{1*fm} > L_{2*fm}$
Uniaxial error	Eccentrically connecting units	$1 * f_m, 2 * f_m$, where $L_{1*fm} < L_{2*fm} \cong 1,2 \dots 1,3 * L_{1*fm}$
	Angular setting error: eccentricity of the axle head bearings	$1 * f_m, 2 * f_m$ where $L_{1*fm} > L_{2*fm}$
Gear drive errors	Eccentric gear tooth connection	$3 * f_Z$ + adjacent channels
	Flank wearing	
	Increase of the gear toothing load	
	Gear gaps	
	Gear tooth breakage	$1 * f_m, 1 * f_o$
	Repetition error	$f_1 = \frac{z_m}{z_m x z_o} f_m, f_2 = \frac{z_o}{z_m x z_o} f_o, 2 * f_1, 2 * f_o$
Mechanical clearances, gaps	Foundation, Bolt connections, bearing clearances	$n * f_m, n * f_o$, where $n = 15 \dots 20$
Bearing errors	Cage frequency	These frequencies are proportional with the rotational speed and depend on the installed bearing's geometrical parameters.
	Inner ring frequency	
	Extern ring frequency	
	Rolling unit frequency	
	Rolling unit rotational frequency	

Vibration-source	Occurrence	Characteristic frequencies [Hz]
Errors derived from cutting process	Catch stepping of the cutting edges	$N * f_o$, where N is the numbers of cutting-edge
	The milling disk	The disk's self-frequency

4. THE DEVICE SYSTEM OF THE INSTRUMENTAL VIBRATION TEST

The oscillation state of the milling machine was tested by vibration pick-up sensors which were placed on the machine's specific points. The positions of measuring points were selected in such a way, that all vibrations from the listed sources in *Table 1* can reach at least one of the sensor with due measurement. Important consideration was composed, that the sensors must been placed directly on the machine frame, ribbing or nearby of that – not on the plating, plate-like parts, bars or servo-mechanism – as close as one of the reviewed oscillation sources, so been supported due efficiency detection of vibrations.

In the course of tests – properly unto the certain vibration sources – displacement and acceleration of vibration diagrams were registered in the following sensor-distribution:

- 1 piece of shift vibration sensor laser interferometer made by Panasonic-SUNX, with *10 kHz* sampling frequency and *4 μm* resolution. By the help of this sensor, partly the environmental vibrations, partly the idling axial direction shift vibrations of the spindle-milling-disk assembly were identified;

- 1 piece of inductive principle seismic sensor made by HBM, which is sensitive along horizontal plane with *1 μm* resolution and *20–120 Hz* frequency range. By the help of this sensor, the feeding-direction horizontal vibrations were determined partly from the environment, partly from the idling state of the equipment, in the first place from imbalance, from the eccentrically rotating machine parts, the deformed shafts, the uniaxial errors and the machining process (*Figure 1,* H);

- 1 piece of inductive principle seismic sensor made by HBM, which is sensitive along vertical plane with *1 μm* resolution and *20–120 Hz* frequency range. By the help of this sensor, the vertical direction shift vibrations caused by excitations were identified from the imbalance, the vertical direction gaps, the machining process and the machine foundation errors (*Figure 1,* V);

- 3 pieces of PIEZO-CUBE g-sensor made by KISTLER, which are sensitive along one axis with *0–8 kHz* frequency range. By the help of these sensors, the acceleration of vibrations were determined from the imbalance, shape and position error, the gear connection, the accidental bearing errors, gaps and the machining process (*Figure 1,* 338, 339, 340).

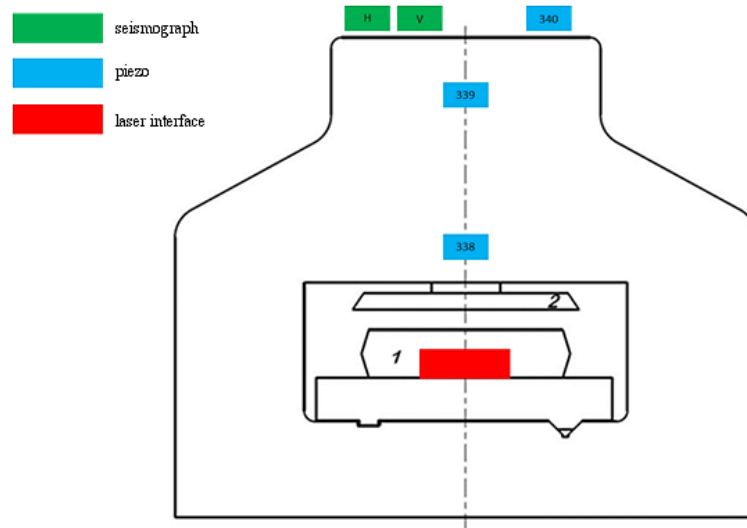The figure below *(Figure 1)* shows the placement of sensors on the machine frame.

Figure 1. The placement of sensors

5. EXAMINATION OF THE ENVIRONMENTAL VIBRATIONS

In doing so, the synergy of environmental oscillations were registered, during measurements, all the sensors worked, the milling machine and its auxiliary units were off. The diagram of *Figure 2* sets an example for the negligible quantity influence of the environmental vibration, which was registered by the horizontal plane sensitive seismograph that was placed on top of the milling-tower and shows the feeding-direction vibration.
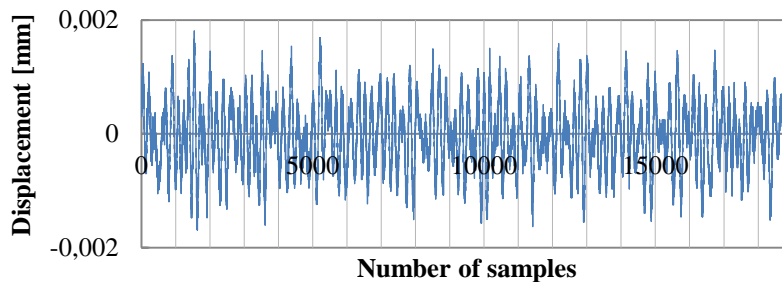

*Figure 2. The feeding-direction vibration of horizontal seismograph (standing)*

Other sensors detected similar negligible vibration level, so it could be pronounced that the influence of the environmental vibrations are not significant, approach in negligible quantity to the oscillation state of the equipment during machining process.

6. IDLE CONDITION

In this state the auxiliary equipment of the milling machine are working, the main spindle with the milling head are running at a given speed, the sledges are not moving and there is no work piece in the working area. With this test we revealed the vibration conditions resulting from eccentrically turning masses, spindle setting, eccentric connections, unbalance, mechanical looseness, unbalance and faults of gears.

6.1. Eccentric parts

Three parts of this kind can be found in the machine: the main spindle, parts turning together with the main spindle and the two driving motor spindles and parts turning together with them. Typical frequencies are $1 \times f_m$ and $1 \times f_o$ *(Table 1)*. The relevant low band vibration and spectrum diagrams can be seen in *Figure 3*.

Figure 3. Vibration and spectrum diagrams
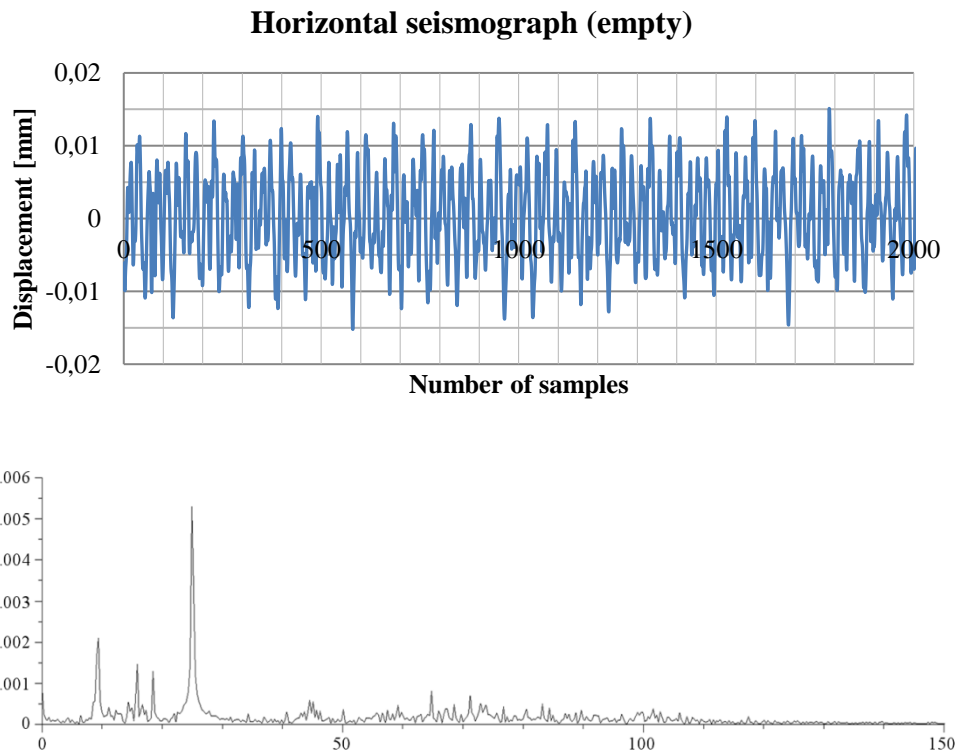
On the low band spectrum diagram we can see that high values appear at the frequencies of the main and driving spindles (*9 Hz* , *25 Hz*), therefore excitation from eccentric rotating parts may be present in the machine.

6.2. Deformed spindles

This vibration source can be originated form the deformity of the driving and main spindles caused by gear connection between the spindles. Typical frequencies are $1 \times f_m$, $2 \times f_m$, where $L_{1 \times f_m} > L_{2 \times f_m}$. Looking at the previous diagram *(Figure 3)* it can be clearly seen that $2 \times f_m$ can be found in negligible amount, thus it slightly influences the machine's condition.

6.3. Eccentrically connecting turning parts

This kind of excitation can be originated from the clutch connecting the spindle of the electric motor and the end of the spindle driving the main spindle. Typical frequencies are $1 \times f_m$, $2 \times f_m$, where $L_{1 \times f_m} < L_{2 \times f_m} \approx 1,2...1,3 \times L_{1 \times f_m}$. This relation cannot be found in the spectrum diagram *(Figure 3),* therefore this factor is unimportant.

6.4. Unbalanced turning masses

Typically appears in the spectrum at equal rotational frequencies equal to revs additively and inseparatively from the presented errors before. Due to the sampling in the low band frequency range we get a result freed from high frequency noises *(Figure4).*
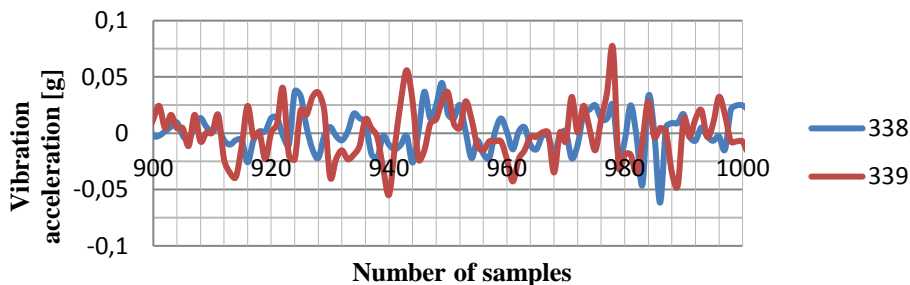

Figure 4. Spindle imbalance

The diagram shows the transmitted signals of vibrations from the accelerometers marked 338 and 339 *(Figure 1),* which were placed at the upper and lower bearings of the main spindle. It is noticeable that the signals run in phase or opposite phase alternatively. This can be allude to floating phenomenon, which can be originated from the processing movement of the main spindle which acts like pendulum with high moment of inertia. It forecasts some types of bearing defects (gaps, wearings). The sources of errors described in *chapters 3.1–3.4* are inducing on frequencies maximum twice as the speed-frequencies present in the machine. These frequencies, except $2 \times f_m$, appears on the spectrum in *Figure 3,* but their absolute signal

level – because of the low band sampling – not so informative. The next diagram shows a much wider – 1200Hz – spectrum range.
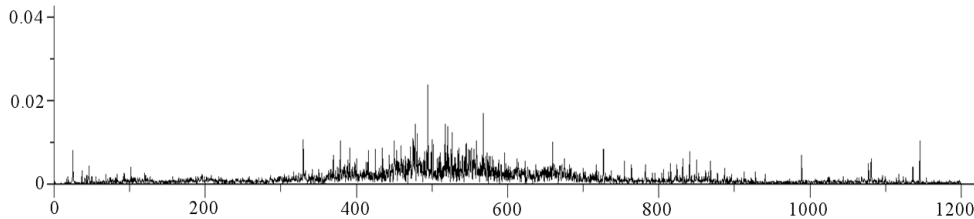

Figure 5. Spectrum diagram

It is clear from the diagram that the 0–1200Hz band signal levels of the spectrum are low compared to the lines in the midrange which are likely bearing noises. So the effect of vibrations from sources of errors described in *chapters 3.1–3.4* does not looks significant to the machine condition.

6.5. Vibrations caused by gear defects

These defects – eccentrically connecting gear pairs, excessive loads on some tooth, gaps between teeth – comes from excited vibrations of the connecting gears of the machine. Typical frequencies $3 \times f_z +$ (the sidebands of the rev. speed of gears), contact frequency: $f_z = z_o \times f_o = z_m \times f_m$, where z_o, z_m the number of teeth on the main and motor spindle. In our case the $z_o = 92$, $z_m = 34$, so the contact frequency is $f_z = 34 \times 25\ Hz = 850\ Hz$, which second harmonics is $3 \times f_z = 2550\ Hz$. The related spectrum diagram *(Figure 6)* was recorded by the closest piezo electric accelerometer – marked 339 – to gears, sensitive in the radial direction to the gears.
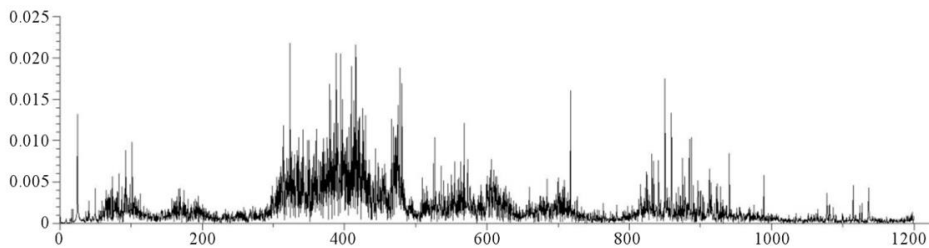

Figure 6. Spectrum diagram

Around $f_z = 850\ Hz$ and $3 \times f_z = 2550\ Hz$ the typical striped lines modulated by the speed frequency of the main spindle can be noticed, which can occur from the increased gap between the teeth of the gears caused by wear of the gears.
Spectrum lines of other gear defects (breakage, repetition error etc.) cannot be found in neither on the recorded vibration diagram, nor it's spectrum *(Figure 6)*.

6.6. Mechanical looseness, fitting gap

This vibration error appears as a result of the loose fitting of bearing elements in this machine. Spectrum lines emerge at the rotational frequency and its multiples of the specific bearing and results in the characteristic fishbone pattern *(Figure 7, Figure 8).*
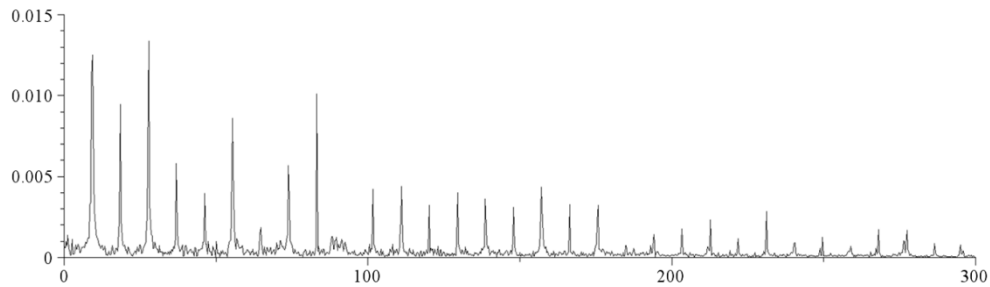

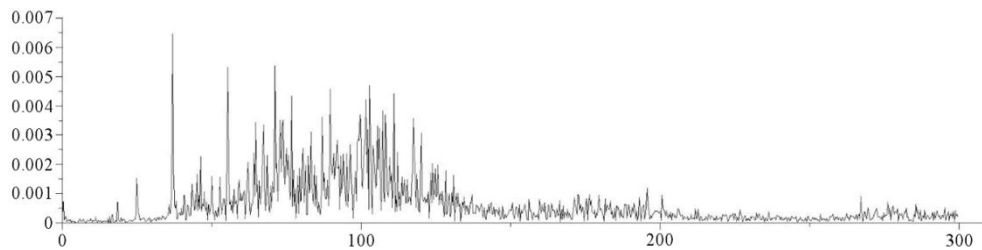*Figure 7. Fishbone patterns of spectrum diagram*

Figure 8. Spectrum diagram

For the recording of these, we used a laser interferometer *(Figure 7)* placed under the milling head targeted to the middle of the cross-section, and piezoelectric accelerometer – marked 340 *(Figure 8)* placed axially on the portal structure. The characteristic fishbone pattern can be observed on both diagrams, which refers to significant axial displacement, verifying the gap in the thrust bearing from constructional reasons. The vibration diagram recorded by the laser interferometer shows 0,08–0,1 mm idle displacement of the main spindle – milling head assembly.

From the spectrum diagrams we think that the axial vibrations caused by the 0,3–0,4 mm prescribed gap for the bearings of the main spindle, have significant impact on the waviness of the surfaces of the aluminium ingot.

7. ANALYSIS OF VIBRATIONS COMING FROM MANUFACTURING

In this chapter we review the effect of machining on the machine-vibration condition. During machining tests we analysed the displacement-vibrations of the top of the machine portal *(Figure 1,* H, V) and the noises of bearings and gears *(Figure 1,* 338, 339, 340) together with the effect of axial bearing gap *(Figure 1,* 340). The

test was conducted at several cutting conditions, we represent our result with the usage of 6000 mm/min feedrate and 8 mm axial depth of cut.

The diagram below *(Figure 9)* shows the displacement-vibrations of the top of the machine structure in feed direction.
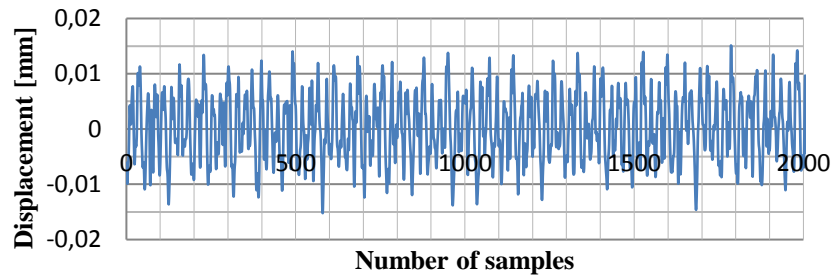

Figure 9. Displacement-vibrations of horizontal seismograph (empty)

Comparing this with the vibration diagram in *Figure 3* it is clear that the examined point of the machine structure doesn't have significant displacement during machining, because the vibrations in the feed direction only slightly increased. We can declare the same about the vertical **v**ibrations of the tower. One likely reason is the gyroscopic stabilizing effect of the main spindle and milling disc assembly, which has a great angular momentum.

Take a look on the recorded vibrations of the "338" piezo electric sensor which was attached near to the lower bearing of the main spindle *(Figure 10)*.
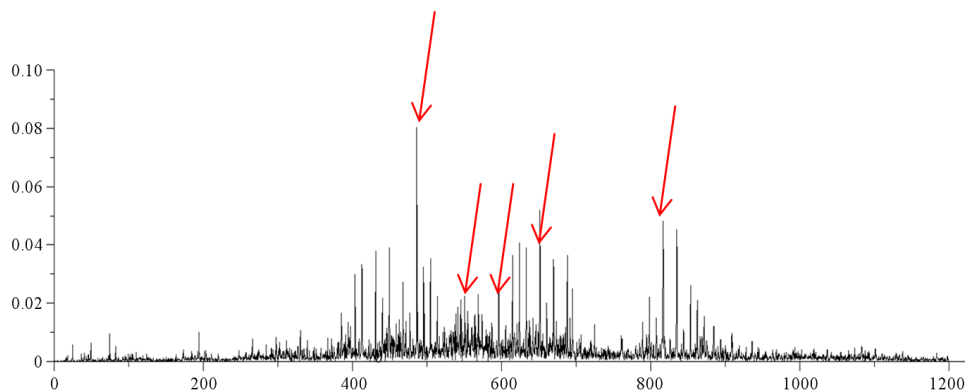

Figure 10. The recorded vibrations of the "338" piezo electric sensor

Comparing this with the idling spectrum diagram of the same sensor, it is obvious, that the spectrum lines of the noises of the lower bearing marks out, which error frequencies can be calculated by knowing the bearing characteristics and by the help of it can be easily identified *(Table 2, Table 3)*. The highlighted frequencies are marked with red arrows in the diagram. The bearing noise – based on the dia-

gram – contributes in a notable way to the vibration condition of the machine during machining, which can prognosticate the significant wear of the affected bearings.

Table 2

Defect frequencies and harmonics of FAG 49/500 NNU type, double row, cylindrical roller bearing

Defect frequency and harmonics [Hz]	1x	…	3x	4x
Rotational frequency	9.083	…	27.249	36.332
Cage frequency	4.265	…	12.795	17.06
Rolling Element Frequency	74.178	…	222.534	296.712
Inner ring frequency	183.11	…	549.33	732.44
Outer ring frequency	162.056	…	486.168	648.224
Rolling frequency	148.355	…	445.065	593.42

Table 3

Defect frequencies and harmonics of FAG 7511-type, angular contact ball bearing

Defect frequency and harmonics [Hz]	1x	2x	…	6x	…	12x
Rotational frequency	9.166	18.332	…	54.996	…	109.992
Cage frequency	4.58	9.16	…	27.48	…	54.96
Rolling Element Frequency	67.6	135.2	…	405.6	…	811.2
Inner ring frequency	192	384	…	1152	…	2304
Outer ring frequency	192	384	…	1152	…	2304
Rolling frequency	135	270	…	810	…	1620

In *Figure 7* we can see the effect of excitation coming from the bearing gap to the machining, which already has been identified during idle run tests. For this observe the spectrum diagram of the "340" accelerometer which was attached in the direction of the main spindle *(Figure 11)*.
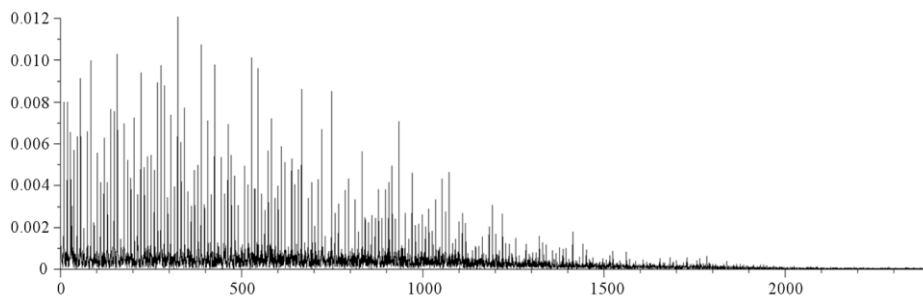

Figure 11. Spectrum diagram

This diagram compared with the idle state spectrum on *Figure 7* shows a typical equidistant, so-called fishbone texture, which obviously refers to the presence of the bearing gap during machining and the clashes from the vertical vibrations of the main spindle.

8. CONCLUSION

From the time and spectrum diagrams of the vibrations recorded during machining, we can draw the conclusions as follows:

- The displacement- vibrations recorded by the seismographs (*Figure 1,* H, V) are slightly increased between idle and machining runs
- The rise of the vibrations recorded by the "338" piezoelectric accelerometer by 100% is due to the increased bearing and gear noises – based on the frequencies – and the excited frequencies of the cutting (primarily from the milling head, like a flexible disc)
- Significant noise is generated by the lower radial cylindrical roller and angular bearings of the main spindle *(Table 2 and 3)*
- The diagram in *Figure 10* suggests that during both idle and machining runs the main spindle assembly has vibration in axial direction with significant amplitude. The detection of the numerical values of this vibration – respect our toolkit – can be conducted with the laser interferometer, but we could only take measurement during idle run by pointing on the appropriate point of the main spindle. During machining we could not use this equipment, so we could only verify it relying on the "340" piezoelectric accelerometer.

On the whole we presume that the 0,3–0,4 mm gap between the lower angular bearings of the main spindle has a major role in the creation of axial vibrations, which are responsible for the increased waviness of the ingot's surface during machining. We describe the theoretical investigation and verification in another article.

REFERENCES

[1] *Tuskómaró forgácsolási paramétereinek fejlesztése.* Kutatási jelentés, 2009. 10. 07.

[2] *Precíziós és nagy pontosságú marási technológia fejlesztése a hengerműben.* Tanulmány, 2010. 04. 30.

[3] *Tuskómaró optimális forgácsolási paramétereinek tesztelése.* Kutatási jelentés, 2010. 07. 23.

[4]   NAGY, István: *Állapotfüggő karbantartás. Műszaki diagnosztika I.* Delta-3N Kft., Paks, 2006.

[5]   DÖMÖTÖR, Ferenc: *Rezgésdiagnosztika I–II.* Dunaújváros, 2008, 2010.

AN OVERVIEW TO CHOOSE THE PROFILE SHIFT COEFFICIENT FOR INVOLUTE GEARING INCLUDING PLANETARY GEAR DRIVES

ZOLTÁN TOMORI[1]–GABRIELLA BOGNÁR[2]

[1]PhD student, [2]professor
University of Miskolc, Institute of Machine and Product Design
3515 Miskolc, Egyetemváros

Abstract: At the beginning of 21th century the literature of involute gear drives describe many different methods for the optimum choice of the profile shift factor. These methods had been worked out for one pair of drives, but leaning on the main principles these can be developed for simple planetary gear drives. At first we review the most significant methods for one pair of gears, then we advert to the methods for planetary gear drives.

Keywords: *Gear, profile shift factor, involute, planetary gear drive*

Nowadays the literature of involute gear drives describe many different methods for the determination of the profile shift factor. These methods had been worked out for one pair of drives, but leaning on the main principles these can be generalized for simple planetary gears. At first we review the most significant methods for one pair of gears, then we advert to the methods for planetary gears.

Literatures are known from the beginning of the 20th century that deals with the methods of increasing the load and lifetime of a gear. BÜCHNER [10] determined, that in the aspect of lifetime the fiction of the teeth is significant. He proves that for the amount of the friction the relative sliding is typical, with taking notice on that the one tooth of the pinion contact i times with the gear. This means that friction loss come forward once on the gear it appears i times on the pinion which is important for wearing. It means that for defining of the tooth correction we have to pay respect for the relative sliding on the pinion multiplied by the gear ratio i.

CSERHÁTI [12] defined the relative sliding by drawing it along the tooth profile. He stated that the sliding maximum wear appears on the top of the gear. He suggested to shorten the top of the bigger gear and to lengthen on the smaller gear.

According to VIDÉKI [39] the sliding velocity is significant for the lifetime. He defined by the use of a general center distance between the gears, if aw>a, the sliding velocity reduces. It is practical to enlarge the center distance until the potential of the teething allow.

DIKER [13], SZENICZEI [32] and BOLOTOVSZKIJ [6] described the sizing for balanced relative sliding by that the biggest values of relative sliding on the two side of the line of action have to be equal. This means that calculated values in the contact limit points are corrected, because the relative sliding in the main point is

zero and increasing hyperbolically. The offset values on the line of action divided by the main point are always on the contact points, either equal or not. Their values can be efficiently lowered by increasing the pressure angle. Moreover at a given pressure angle the two biggest sliding can be equalized and minimized.

COLBOURNE [11] worked out a calculating method for internal gears, where the tooth thickness of the external gear is increased to the previously calculated value by a correction factor, while the tooth thickness at the pitch circle of the inner gear is lowered by this factor. The correctional factor is determined to avoid the interferences with the geometry defined by the modified tooth thicknesses.

YU [42] draws attention to that data of the cutting tool have to be known during the design of an internal gear, because after a sharpening the outer diameter of the tool is decreased, the profile shift factor also decreases. If this change is disregarded at the definition of the geometric data of the internal gear, interference can happen during operation or manufacturing.

BOTKA [8], [9] patented in 1954 the Ganz–Botka gearing system. He had shown that if the relative sliding is equalized at the limit contact points, there is triple equalization. It means that beyond the relative sliding, the momentary contact temperature increasing or flash and the two-factor Almen product (products of the Hertz stress and sliding velocity) are also equalized and minimized. He stated that at lower contact angles the temperature increase of the tooth faces are the biggest at the contact limit points. By increasing the contact angle the heat gets its maximum at the contact limit points. In this case he aimed to equalize these heat pitches.

Based on these result Botka found that it is only recommended to use heat equalized gearing when the gear drive has a tendency to seize. In other cases the equalization if relative sliding is the effective method, moreover the root strength is higher. It is especially true for open drives and slow running, heavy loaded drives which are tend to wear faster. At high running speed it is also recommended to use this method instead of the heat equalization, if scoring is not likely to happen.

GAVRILENKO [19] suggested to define the profile shift factors by the equalized relative sliding accelerations, because the relative sliding method has a fundamental problem. Namely at the main contact point the relative sliding is zero, which leads to that there is no wear in turn at the roots should be significant wear. At the same time the practice doesn't confirm this theory. Therefore the places and extents of wear can be determined by the relative sliding acceleration, that is the tangent of the line of act and the sliding curves. In other words the places of wear and pitting should be determined by the changing of the derivative of the relative sliding along the line of action. The best results can be achieved by equalizing the relative sliding accelerations at the contact limit points.

By the studies of NIEMANN [28] stated that the scoring safety factor is optimal when the slip velocities are equal at the contact limit points. It means that the addendum contact numbers are equal. So if these numbers are equal that means the sliding velocities are also equal.

BLOK [4] found during his test about scoring of gears, that happens at high local temperatures. It comes from the difference of the temperature of the gear body and

the local temperature increase at the contact spot. Scoring happens when the sum of the temperature of the gear body and the local temperature increase pass the so called scoring temperature of the lubricant. The seizure temperature can be determined experimentally. The local temperature increase can be determined by the differential equations created by the author, which can be used to define the contact temperatures of the contact points. In this way the optimal dimensions can be defined for the scoring safety knowing the critical temperature of the lubricant.

WINTER [41] created the universally applicable so called integrated temperature criteria method used to define the scoring toughness, based on the works of Blok and Niemann. The main principle of this is that the heat stress is defined by the sum of the temperature of the gear body and the local temperature increase which is considered to be permanent during the line of action. There is no scoring threat if the forming temperature is lower than the experimentally defined temperature which is based on the lubricant, the material of the gear and the loading conditions. With this calculations the optimal dimensions can be defined in the aspect of optimal scoring conditions, but it can be hardly used for the definition of profile shift factors.

TERAUCHI et al. [33], [34] performed experiments on a gear test equipment with closed power flow. At the contact region they achieved the EHD (elasto-hydrodynamic) lubrication and then they seek the optimal parameters for the profile shift factor which gives the best results for the scoring safety. They stated that slightly positive values causes significant improvement. The defined the critical face temperature independently from the lubricant and the material of the gear, where the value of the scoring safety factor is the highest. They determined that the scoring safety can be estimated by the critical face temperature, thus they defined the profile shift factor which causes this critical temperature.

KOLONITS [22], [23] made a computer program for the Ganz–Botka gearing to get the thermal equalization. He uses the newest, mainly Japanese literature which models the heat formation and distribution. He worked out a model similar to the Blok theory, but simpler than the Japanese model. This give adequate results for the industry.

LI–CHIOU–CHANG–YEN [26] made a computational method where during the design of gears using FEM analysis. There they use the pressure angle and the clearance using as parameters get the optimal dimension for the longest lifetime minimizing the Hertz stress.

PEDERSEN–JORGENSEN [29] define the dimensions of a gear be FEM analysis so that the root has as much stiffness as possible. They show that in this way can be achieved the maximum load which means the longest lifespan at given conditions.
KINCZEL [21] examined the straight involute gears in his paper. His work deals with the pairing of the machining and computing methods in details. After the summary of profile shift factor defining methods the author concluded that the refinement of tooth profiles needs the refinement of the correctional methods. By bringing in the universal correctional principle it can be able to get a correct profile

shift factor by using arbitrary friction coefficient and line pressure function. Moreover it tells which kind of correctional factor should be used.

Starting from the general principle (using symmetric linear line pressure and permanent friction coefficient along the line of act) the examination of specific friction energies – in parity with the results of Kolonits – lead to Botka's theory. Furthermore he proved that, there is a pressure angle, at which, using relative sliding equation, the specific friction energie has a minimum. But this minimum is only the 60…30% of the compensated gearing. This pressure angle range is between 24° and 27°.

BAGLIONI–CIANETTE–LANDI [2] worked out a method by defining the slip velocities to improve the efficiency. The proved that by lowering the sliding velocities, the noise, the wear and the performance degradation are also lowering. They made recommendations for choosing the profile shift factor to get the best efficiency.

IMREK–UNUVAR [20] verify the relationship between the tooth profile, the sliding velocity along the line of action, the line pressure and the flank temperature increase. They stated that the driving gear has to made with positive shift factor, while the driven gear with negative shift factor, to get the sliding velocity equalized at the limit contact points. This ensures the smallest value also and minimum wear. TERPLÁN [36], [37] worked out a calculating and constructing method for the compensated teething of planetary gears. He proved that if we sizing for equalized relative sliding and using ordinates at the limit contact points, the problem of fourfold equalization can be reduced threefold.

With his collaborators (SZOTA–SCHOLTZ) worked out a simpler method based on the VÖRÖS [40] method for the construction of the relative slidings of a planetary gear. The calculation method is iterative which solves the problem of the threefold equalization numerically. It is advantageous to use this method to define the profile shift factors because it is simple and clear. He summarized the values of relative slidings and shift factors in tables [36], [37].

APRÓ [1] found out by examining the planetary gears with on degree of freedom, that by reducing the number of teeth of the planet gear general gearing can be used when the energy-flow is the following: sun gear-arm, fixed ring gear. The main principle of the method was that holding the good contacts it is practical the improvement of external contact which can be achieved by reducing the number of teeth. He summarized in tables the reduction of the number of teeth of the planet gear depending on the sum of teeth on the sun and planet gears and the pressure angle.

BOLOTOVSZKIJ [5] examined the teeth correctional factors planar and spatial limiting contours. These contours are created in the coordinate system of profile shift factors by using the different interference equations as limiting function which create there surfaces. These surfaces are used as limits for the interference free zone. If the sun gear and the planet gear contact is equalized for relative sliding in the defined area, than the profile shift factor for the ring gear can be determined with an equation similar to the collinear assumption of the planetary gear.

In literature, beside the general solution of external contact, the following recommendation can be found for the profile shift factor of the ring gear:
According to BERGSTRÄSSER [3] the definition of the profile shift factor of the ring gear, after the definition of sun and planet gears as DIN 3992, are the following:

$$x_3 \cdot m = B_{32} \cdot a_w + x_2 \cdot m, \tag{1}$$

where the B_{32} parameter is the Kutzbach involute function:

$$B_{32} = \frac{inv\alpha_{wt32} - inv\alpha}{tg\alpha}, \tag{2}$$

in which the α_{wt32} pressure angle of the outer-inner contact and α is the standard presssure angle.

RICHTER [31] defines the profile shift factors for external meshing according to DIN, but uses the following equation for the ring gear:

$$x_3 = x_1 + 2x_2. \tag{3}$$

KUDRJAVCEV [24] gave the same equation as Richter for the profile shift factor of the ring gear, but defines the profile shift factors of the external contact by the equalized relative slidings method.

SUMMARY

We can see that the determination of the profile shift factor is as comprehensive as the widespread of the usage of gears. We can settle also that there is no universal method for the determination of the profile shift factor, which only can ensure the best efficiency and longest lifespan for gears at the same time. Accordingly it is recommended to examine the literature carefully for the specific problem and find the best solution for the given conditions.

ACKNOWLEDGEMENT

REFERENCES

[1]   APRÓ, F.: *Egy szabadságfokú fogaskerék-bolygóművek tervezésének néhány kérdése.* Kézirat. Az NME Gépészmérnöki Karára benyújtott és elfogadott egyetemi doktori értekezés. Miskolc, 1967.

[2]   BAGLIONI, S.–CIANETTI, F.–LANDI, L.: Influence of the addendum modification on spur gear efficiency. *Mechanism and Machine Theory,* 49, (2012) 216–233.

[3] BERGSTRÄSSER, M.: Planetengetriebe mit auswechsebarer Übersetzung. *Maschinenbautechnik,* 10, 4 (1961), 209–211.

[4] BLOK, H.: Les températures des surface dans des conditions de graissage sons pression extreme. *Second World Petroleum Congress.* Paris, June 1937.

[5] BOLOTOVSZKIJ, I. A.–GURJEV, B. I.–SZMIRNOV, V. E.–SENDEREJ, B. I.: *Cilindricseszkije evolventnije zubcsatie peredacsi vnutrennova zacaplenyija.* Masinosztrojenie, Moszkva, 1977, 135–144.

[6] BOLOTOVSZKIJ, I. A.–BOLOTOVSZKAJA, T. P.–BOCSAROV, G. Sz.–GURJEV, V. I.–KURLOV, B. A.–MERKURJEV, I. A.–SZMIRNOV, V. E.: *Szprovocsnik po geometricseszkomu raszcsotu evolventnih zubcsatih i cservjacsnih peredacs.* Masgiz., Moszkva, 1963, 24–40.

[7] BOTKA, I.: *Egységes magyar homlokkerék fogazási rendszer.* Mérnöki Továbbképző Intézet, Budapest, 1953.

[8] BOTKA, I.: Fogaskerék-méretezés kiegyenlített kontakt-hőmérsékletre. *Gép,* 16. évf. 1964. 11. szám, 425–430.

[9] BOTKA, I.–ERNEY, Gy.: *Fogaskerékpárok méretezése. Egyenes fogazat.* Akadémiai Kiadó, Budapest, 1973, 14–23.

[10] BÜCHNER, K.: Beitrag zur kenntnis der Abnutzungs- und Reibungsver-hältnisse der Strinzahnräder. *Zeitschrift des VDI,* Nr. 5. Februar 1902, 159–166, 278–284.

[11] COLBOURNE, J. R.: The geometric deisgn of internel gear pairs. *Gear Technology,* May/June 1990, 28–37.

[12] CSERHÁTI, J.: *Gépelemek.* Egyetemi jegyzet, amelyet készített Vidor J. Rezső. é. n. 53–56.

[13] DIKER, J. I.: *Evolventnije zaceplenyije sz uprjamimi zubcami.* Organyetall, 1935.

[14] DIN 3992.

[15] DROBNI, J.: *Hajtóművek Gépszerkezettana II.* c. egyetemi előadásai az NME Gépészmérnöki Karán a Géptervező Szak Általános Gépészeti Ágazatos hallgatóinak az 1980/81-es tanévben.

[16] DROBNI, J.–SZENTE, J.–GÓDOR, I.: Belső fogazatú fogaskerékpár csúszási sebességének kiegyenlítése. *NME Közleményei III. sorozat. Gépészet,* 27. Miskolc, 1981.

[17] DROBNI, J.: *Metszőkerék tervezése belső fogazatú fogaskerékhez.* Tervezési segédlet. Gé. 79-2067. NME, Miskolc, 1979, 10–29.

[18] ERNEY, Gy.: *Fogaskerekek.* Műszaki Könyvkiadó, Budapest, 1983, 5. fejezet.

[19] GAVRILENKO, V. A.: *Osznovi teoriji evolventnoj zubcsatoj peredacsi.* Masinosztrojenie, Moszkva, 1966, 234–245.

[20] IMREK, H.–UNUVAR, A.: Investigation of influence of load and velocity on scoring of addendum modified gear tooth profiles. *Mechanism and Machine Theory,* 44 (2009), 938–948.

[21] KINCZEL, F.: *Egyenes fogú evolvens fogazatú hengeres kerékpárok fogazathatárai és fogazathelyesbítése.* Kézirat. Az NME Gépészmérnöki Karára benyújtott és elfogadott műszaki egyetemi doktori értekezés. Miskolc, 1975.

[22] KOLONITS, F.: Hőfokvillám-kiegyenlítés egyenes fogú evolvens kerekeken. *Műszaki Tudomány,* 49. 1975. 353–370.

[23] KOLONITS, F.: Fogaskerék-villámhőmérséklet II. A változó kapcsolódási viszonyok hatása. *Műszaki Tudomány,* 52. 1976. 183–198.

[24] KUDRJAVCEV, V. N.–KIRDASEV, Ju. N.: *Planetarnije Peredacsi.* Masinosztrojenie. Leningradszkoje otdelenyije, Leningrad, 1977, 137.

[25] LÉVAI, I.–SZARKA, Z.: D-függvény a fogaskerekek geometriai méretezéséhez. *NME Gépelemek Tanszékének Közleményei,* 203. sz. Miskolc, 1969, 1–23.

[26] LÍ, C. H.–CHIOU, H. S.–HUNG, C.–CHANG, Y. Y.–YEN, C. C.: Ingegration of finite element analysis and optimum design on gear systems. *Finite Elements in Analysis and Design,* 38 (2002), 179–182.

[27] LITVIN, F. L.: *A fogaskerékkapcsolás elmélete.* Műszaki Könyvkiadó, Budapest, 1972, 226–238.

[28] NIEMANN, G.: *Maschinenelemente.* Band II. Springer Verlag, Berlin (Göttingen)– Heidelberg, 1965.

[29] PEDERSEN, N.–JORGENSEN, F. J.: On gear tooth stiffness evaluation. *Computers and Sturctures,* 135 (2014), 109–117.

[30] POLDER, J. W.: Overcut interference in internal gears. *International Symposion on Gearing and Power Transmissions.* Tokyo, 1981.

[31] RICHTER, W.: *Auslegung von innenverzahnungen und Plametengetrieben Kostruktion.* Bd. 14, Nr. 12 (1962), 489–497.

[32] SZENICZEI, L.: *Az általános fogazás.* Királyi Magyar Egyetemi Nyomda, Budapest, 1941, 135–148.

[33] TERAUCHI, Y.–NADANO, H.: Effect of tooth profile modification on the scoring resistance of spur gear. *Wear,* Vol. 80, No. 1 (1982), 27–41.

[34]   TERAUCHI, Y.: Scoring of spur gear teeth. *Lubrication Engineering,* Vol. 40, No. 1 (1984), 13–20.

[35]   TERPLÁN, Z.–APRÓ, F.–ANTAL, M.–DÖBRÖCZÖNI, Á.: *Fogaskerék-bolygóművek.* Műszaki Könyvkiadó, Budapest, 1979, 17–19, 92–104.

[36]   TERPLÁN, Z.: *Gépelemek II.* Kézirat. Tankönyvkiadó, Budapest, 1981, 26–28.

[37]   TERPLÁN, Z.: *A fogaskerék-bolygóművek méretezési kérdései.* Kézirat. A TMB-hez benyújtott és elfogadott akadémiai doktori értekezés. 1965, 39–54.

[38]   TOMORI, Z.: Relatív csúszásra optimalizált kb típusú fogaskerék-bolygóművek számítógépes tervezése. *Géptervezők VI. Országos Szemináriuma.* Miskolc, 1985.

[39]   VIDÉKI, E.: *Fogaskerekek.* „Pátria” Irodalmi Vállalat és Nyomdai Rt., Budapest, 1912, 94.

[40]   VÖRÖS, I.: *Gépelemek III. Fogaskerekek.* Tankönyvkiadó, Budapest, 1956, 101–121.

[41]   WINTER, H.–RICHTER, M.: Verzahnungswirkungsgrad und Fresstragfähigkeit von Hypoid- und Schraubenradgetrieben. *Antriebstechnik,* Bd. 15, Heft 4 (1976), 211–218.

[42]   YU, D. D.: On the interference of internal gearing. *Gear Technology,* July/August 1989, 12–44.

THE USEABLE SECTION OF PROFILE SHIFT COEFFICIENT

ZOLTÁN TOMORI[1]–GABRIELLA BOGNÁR[2]

[1]PhD student, mechanical engineer, nordker94@t-online.hu
[2]professor, v.bognar.gabriella@uni-miskolc.hu
University of Miskolc
Institute of Machine and Product Design
3515 Miskolc-Egyetemváros

Abstract: The basic aim of this paper is to determine the possible limits of profile shift coefficient. Another interesting problem is the behaviour of the limit. The paper interprets that the limits are absolute ones, because the geometrically correct tooth profile can be produced only between the limits.

Keywords: *undercut, zero topland, profile shit coefficient limits*

1. INTRODUCTION

During the design of a gear pair, especially in the geometrical predesign we define the number of teeth, the module of the gears and the working centre distance of axles. By defining the working centre distance, which is not equal to the standard centre distance, we define the sum values of the profile shift coefficients also.

In view of the sum of profile shift coefficients and by the usage of various methods, the profile shift values for each gear can be calculated. For example by equalizing the relative sliding in the end points of meshing or by the values of flash temperature in the same points etc. [1], [2].

In this paper we analyse if these profile shift coefficients have an upper and lower limits and if they have what is it?

We made our test on involute spur gears machined by straight edged tool. The results can be expanded to spur and helical gears made by shaper cutter.

The value of profile shift coefficients shows that the distance between the centre line of the cutting tool and the pitch line, the profile shift value is how many times of the module. The indication shows the direction of shift.

With this in mind if we shift the cutting tool towards the centre of the machined gear, from the machining position of the standard toothing to the centre point the value will be negative.

If we move it in the other direction, or pulling it out, than the value will be positive.

Examine that if this movement of the cutting tool has any limits.

2. THE UNDERCUT

It is known that the start points of the involute profiles of the gear are lying on the base circle and the involute profiles starting from this points are lying on a larger circle than the base circle. The involute profile points can not be made on a circle what has smaller radius than the base circle.

At first examine the tip of the cutting tool, because this part of the tool gets the closest to the centre point of machined gear.
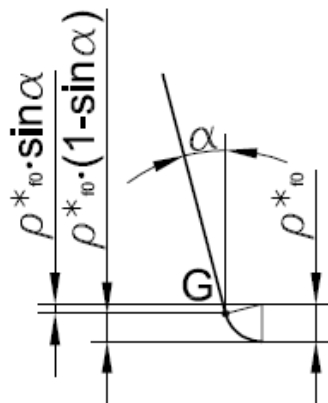

Figure 1. The rounding of the tool edge

As it can be seen on the first figure, the G point is the limit point belonging last to the straight line of the edge. Going on the tool edge to the tip, the rounding comes next, which cannot be used for making involute profile because it is not part of the straight profile. This rounding forms the bottom radius of the tooth, which is not involute.
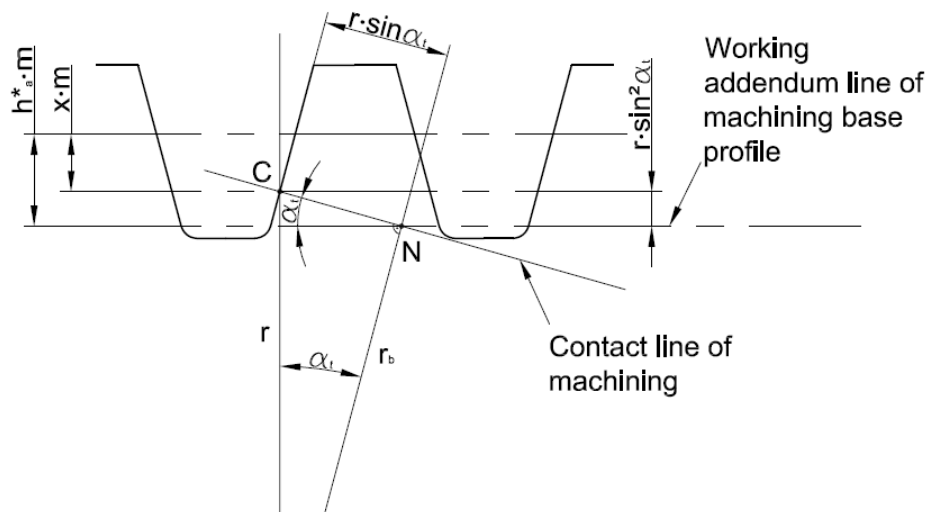
Figure 2. The limit of the base profile

The second figure shows the border-line case, when the working top line crossing the limit point *N* of the gear. The last point of the straight profile on the cutter useable to make involute profile, when it crosses the base point *N* on machined gears.
In this position the distance between the working top line of the tool and the centre point of the machined gear is smaller than the radius of the base circle of the gear. Thus the points near the tip of the tool are cutting on the area where involute profiles cannot be made on the gear blank. In this case during the roll out of the tool, the cutting edges are cutting parts of the useable profiles made during roll in [3]. It is called machining interference or undercut.

Using the notation on the *Figure 2.* it can be written, when there are no undercut, like in the limit case shown on the figure:

$$(h_a^* - x)m = r\sin^2\alpha_t = \frac{m\,z}{2}\sin^2\alpha_t. \tag{1}$$

So

$$x_{min} = h_a^* - \frac{z\sin^2\alpha_t}{2}. \tag{2}$$

From the *Equation (2)* the minimal value of the profile shift coefficient can be determined in every machined gear, when undercut just not happen.

Using smaller values than this causes undercut, that is the lower limit of the determined value which gives accurate tooth profile.
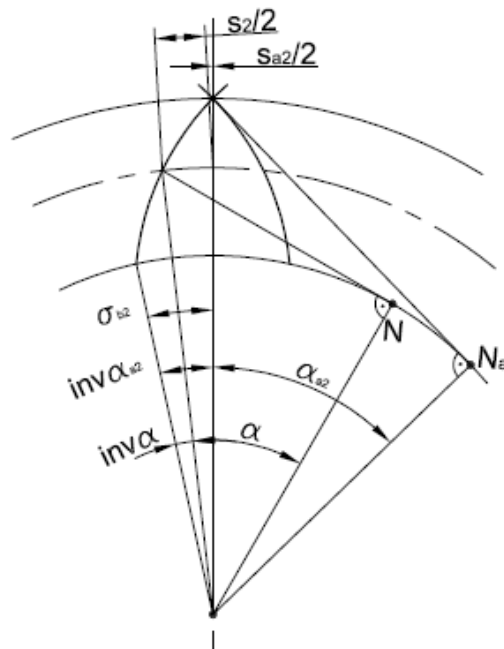
3. ZERO TOPLAND

Figure 3. The phenomenon of the tooth thickness

Next examine the geometrical relations when the cutting tool is „pulled out", when the profile shift coefficient has a positive value, respectively is it have a limit value?

As it is shown on the *Figure 3.* the tool by pulling outside, receding from the centre point of the machined gear, we make the farther points of the elemental involute profile [4]. In a border-line case it can happen that we would make that area where the two involute arcs crosses each other. In this case during the rolling out of the tool, the cutting edges machines down the profiles on a larger circle than the circle lies on the intersection point of the two tooth sides. This phenomenon called another machining interferences, tip relief.

In practice the minimal topland thickness have to be granted, because if it grows thin it causes strength problems. In literature the minimal value related to the module is advised to pi ck up between $s_{amin}^* = 0{,}2 \ldots 0{,}3$. By using the nomenclature on *Figure 3* we can define the minimal topland thickness by the following equation:

The tooth thickness on the pitch circle from the figure is:

$$s = \frac{p}{2} + 2xm \tan\alpha \tag{3}$$

where *p* is the pitch on the pitch circle, *m* is t he module, *x* is the profile shift coefficient, while α is the pressure angle of the profile.

The angle σ_a belonging to the profile can be determined:

$$\sigma_a = \frac{s}{2r} + inv\alpha = \frac{s_a}{2r_a} + inv\alpha_a. \tag{4}$$

Based on these equations the thickness on the topland is:

$$s_a = 2r_a \left(\frac{s}{2r} + inv\alpha - inv\alpha_a \right) \tag{5}$$

By substituting the tooth thickness and the profile angle belonging to the addendum circle, the topland thickness is:

$$s_a = d_a \left\{ \frac{\pi}{2z} + \frac{2x}{z} \tan\alpha + inv\alpha - inv \left[\arccos \left(\frac{zm}{d_a} \cos\alpha \right) \right] \right\} \tag{6}$$

which cannot be smaller than the s_{amin} value given earlier.

In regard to that *Equation (6)* is transcendent to *x*, so defining x_{max} can be done by using some numerical method, by the presumption, that the value of the left side of *Equation (6)* is equal with s_{amin} selected from the literature.

Since the tip relief happens on that diameter when the two involute profiles cross each other, namely when the rolling out tool cuts off the profile made during roll in, on bigger diameter than this involute profile cannot be made.

4. EXAMPLE

For the limit values shown in this paper, we present the next sample without the detailed calculations:

Basicdata

Number of teeth of thegears	$z_1 = 19$	$z_2 = 35$
Module	$m = 3\ mm$	
Centre distance	$a_w = 83\ mm$	
Pressure angle	$\alpha = 20\ fok$	
Addendum factor	$h_a^* = 1$	
Clearance factor	$c^* = 0{,}25$	

Calculations

Base pitch	$p_b = 8{,}856\ mm$	
Base circles radii	$r_{b1} = 26{,}781\ mm$	$r_{b2} = 49{,}334\ mm$
Working pressure angle	$\alpha_{wt} = 23{,}502\ fok$	
Sum of profile shift coefficients	$\Sigma x = 0{,}724$	
Standard centre distance	$a = 81\ mm$	
Centre distance coefficient	$y = 0{,}667$	
Minimum values of profile	$x_{1min} = -0{,}111$	
shift coefficients	$x_{2min} = -1{,}04$	
Limit of topland	$s_{amin} = 0{,}3{\times}3\ mm$	
Maximum values of profile	$x_{1max} = 0{,}894$	
shift coefficients	$x_{2max} = 1{,}401$	

The obtained results are represented by the $x_2 = f(x_1)$ function with the limits in the x_1, x_2 coordinate system shown in *Figure 4*.
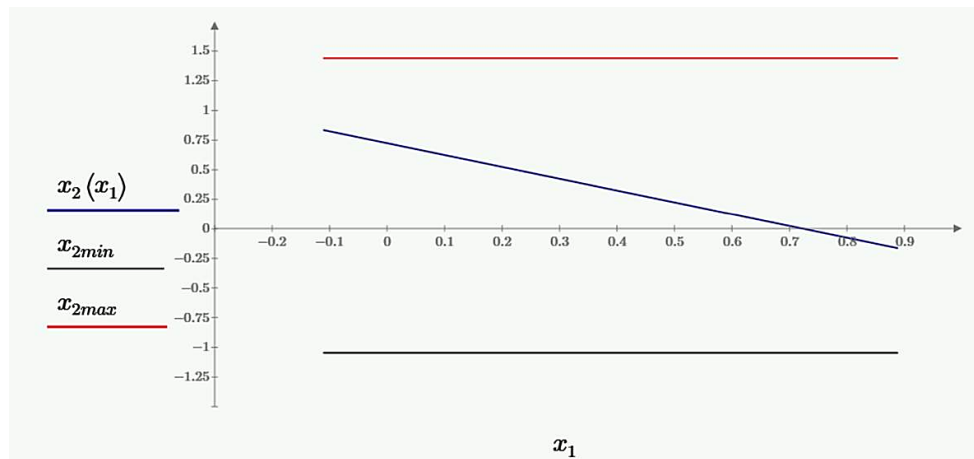
Figure 4. Relation of the profile shift coefficients with their limits

5. CONCLUSIONS

1. The domain of the profile shift coefficients can be defined on every machined gear with the minimum and maximum values, where geometrically correct involute profile can be made.
2. The upper and lower limit of this domain obtained, are critical values from the perspective of the geometrically correct tooth profile, because beside these limits geometrically correct involute profile on the given gear cannot be made.

REFERENCES

[1]   COLBOURNE, J. R.: *The geometry of involutegears.* Springer-Verlag, New York, 1987.

[2]   ERNEY, György: *Fogaskerekek.* Műszaki Könyvkiadó, Budapest, 1983.

[3]   JELASKA, D.: *Gears and geardrives.* John Wiley&Sons Ltd., Chichester, 2012.

[4]   KAPELEVICH, A. L.: *Directgear design.* CRC Press, BocaRaton, 2013.

ROLLING BEARING FATIGUE TESTS USING STATISTICAL PARAMETERS

DÁNIEL TÓTH

University of Miskolc, Department of Machine Tools
3515 Miskolc-Egyetemváros
toth.daniel@uni-miskolc.hu

Abstract: The condition monitoring of roller bearings is particularly an important topic nowadays. These machine elements can cause great damages in the most of rotating machineries, therefore perpetual failure detection is necessary. The following paper presents rolling element bearing fatigue tests.

Keywords: fatigue test, vibration analysis, rolling element bearing

1. INTRODUCTION

Rolling element bearings are one of the most widely used machine elements. Their usage means risk for almost all forms of rotating equipment, such as pumps, machine tools, electric motors, generators, starters etc. Their operating properties impact the function of the whole machine [1].

An accidental bearing failure can cause serious damages. In order to hinder abrupt losses, rolling element bearing failures should be detected as early as feasible. Owing to the early detection, availability of machines can be increased. Perpetual condition monitoring facilitates to determine the location of the fault. Thus corrective activity can be taken and maintenance work can be planned properly.

2. CONDITION MONITORING METHODS

Condition monitoring is one possibility of prognostic maintenance programmes. The gathered information can be used to define machinery problems and corrective actions can be implemented. Several techniques are used for detection of bearing failures. These techniques can be classified as temperature monitoring, noise analysis, vibration analysis, wear debris detection etc. Vibration signals collected from rolling element bearings carry detailed information on machine health conditions. Different vibration analysis methods exist to analyse the bearing vibrations. These methods can be categorized into time domain, frequency domain, time-frequency domain and other techniques [2].

Time domain analysis is the most appropriate to random signals, where other signal analysis methods are not applicable [3]. This technique facilitates fast data processing and computation. Various statistical parameters can be applied as trend

parameters to detect the incidence of bearing failures. The most frequently used stochastic indexes are kurtosis, root-mean-square (RMS) value, peak value, skewness, standard deviation, impulse factor and crest factor.

3. BEARING TEST RIG

At laboratory conditions a test machine is necessary to perform bearing condition monitoring. Such a machine is located at University of Miskolc, Department of Machine Tools. This device is used to fulfil the bearing fatigue and measurement examinations. The equipment with its major engineering parts is illustrated in *Figure 1.*
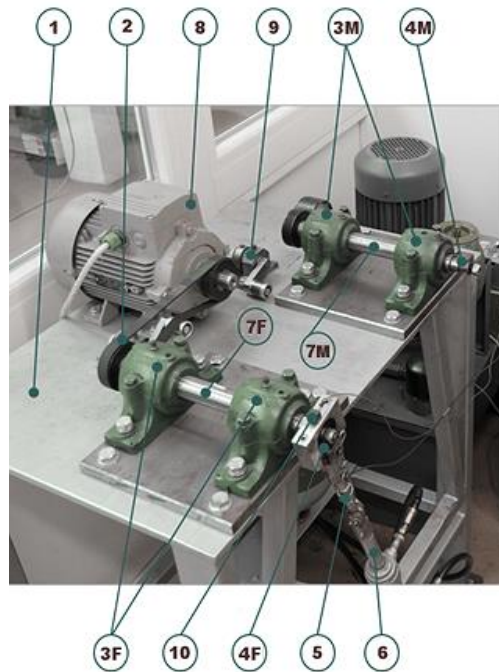
Figure 1. Bearing test machine

Symbols have the following meanings:
- 1:   rigid table,
- 2:   length ribbed belt,
- 3F: supporting bearings of fatigue side,
- 3M: special supporting plain bearings of measurement side,
- 4F: fatigued bearing,
- 4M: measurement position,
- 5:   load cell, the adjustment of hydraulic load,
- 6:   double-acting hydraulic cylinder,
- 7F: fatigue test shaft,
- 7M: measurement test shaft,

- 8:   three-phase motor,
- 9:   belt tensioner,
- 10:   piezoelectric vibration accelerometer.

During bearing fatigue tests the fatigue test shaft (7F) works at the given rotational speed (1500 min^{-1}), while the hydraulic cylinder (6) exerts artificial load (6 kN) for the bearing (4F). After the fixed-term fatigue cycles, the examined bearing is put over to the measuring axis (7M). During the measurement investigations the shaft works (7M) at the given rotational speed (1500 min^{-1}), while the hydraulic cylinder (6) exerts artificial load (1 kN) for the examined bearing (4M).

4. EXPERIMENTS AND ANALYSIS

The experimental analysis of rolling element bearings is carried out on different ways. One method is creating artificial defect on the element of bearing. In this instance the vibration signal is being measured and compared with the data of faultless bearings. Another technique is the fatigue test when bearings operate until they get damaged. Although, the process takes relatively long time, nevertheless it can be accelerated by increasing the rotational speed and load. This study focuses on bearing fatigue tests, a 6303 type, single row, deep groove, ball bearing was analysed.

During the tests, vibration patterns were measured from the examined bearing using Kistler 8632C50, piezoelectric vibration accelerometer. The measurement cycles are performed at 9600 Hz sampling frequency. 16,384-element samples were taken within each measurement cycle. The fixed-term fatigue cycles were about 3-4 hours long. After the fixed-term fatigue cycles, vibration patterns were taken from the bearing and time-domain tests were done during which stochastic indexes have been calculated. The statistical features can be calculated by using the formulas below *(Table 1)*. These indexes were computed by a program code, which runs in Maple software.

Table 1
Calculation of statistical parameters [4]

Kurtosis	$\dfrac{\sum_{i=1}^{N}(X_i - \bar{X})^4}{(N-1)S^4}$
Peak Value	$\dfrac{1}{2}\left(max(x_i) - min(x_i)\right)$
Root mean square	$\sqrt{\dfrac{\sum_{i=1}^{N}(x_i)^2}{N}}$
Standard deviation	$\sqrt{\dfrac{\sum_{i=1}^{N}(x_i - x_m)^2}{N-1}}$
Skewness	$\dfrac{\sum_{i=1}^{N}(X_i - \bar{X})^3}{(N-1)S^3}$

In the formulas, N is the number of discrete points, $\bar{x}$ is the value of the discrete time signal, x_i is the i-th test sample.

Kurtosis value is a non-dimensional stochastic index. This indicator is compromise measure between the intensive lower moments and other susceptible higher moments. Peak value is the disparity between the maximum negative and the maximum positive amplitudes. RMS measures the comprehensive level of discrete signal.

The temporal dependence of the statistical index is usually called lifetime curve. *Figure 2* depicts the Kurtosis value.
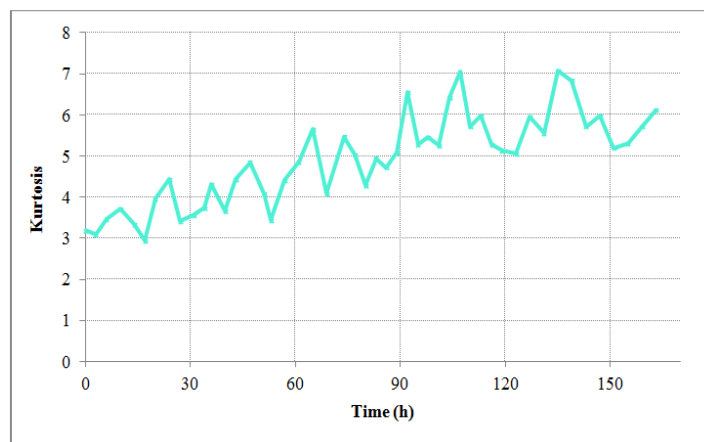
Figure 2. Kurtosis history of vibrations

It is visible that Kurtosis correlated well. The values not increased significantly after 90 hours. In *Figure 3* the peak value change is shown.
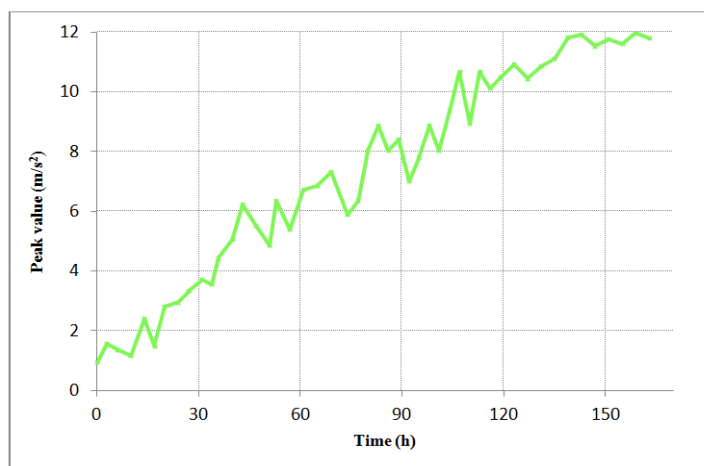
Figure 3. Peak-to-peak value history

It is clearly visible that acceleration values increased continuously by passage of time. It is apparent that it has good correlation. *Figure 4* shows the change of root mean square. The trend of RMS graph seems somehow similar to the peak graph.
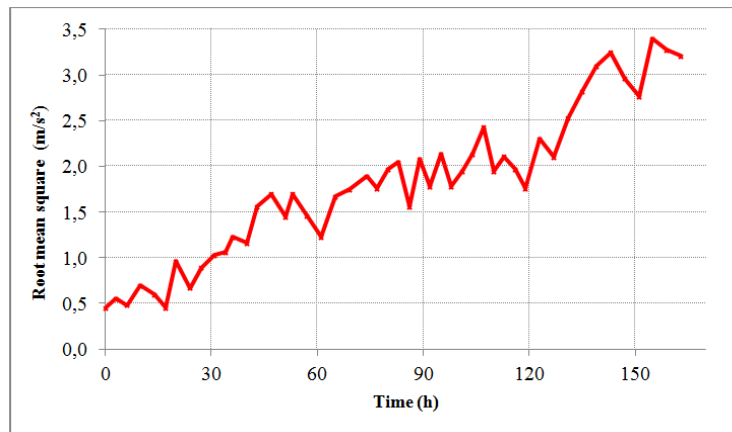

Figure 4. Root mean square value as a function of time

There is a sudden growth in the graph, at around 130–150 hours. At this time the bearing noise had increased, which can caused by exhaustion of the bearing. When the bearing exceeded its nominal lifetime, it was disassembled. As the analysis predicted, the bearing had a defect after 160 fatigue hours. The main reason of bearing failure was the cage failure, which could be caused by heavy loads.

5. CONCLUSION

This paper shows that vibration analysis methods, especially time domain techniques can be perfectly used in condition monitoring of roller bearings. Statistical analysis methods are accurate tools and they make possible quick data processing.

ACKNOWLEDGEMENT

REFERENCES

[1]   KIM, P. Y.–LOWE, I. R. G.: A review of rolling element bearing health monitoring. *Proceedings of Machinery Vibration Monitoring and Analysis Meeting.* Vibration Institute, Houston, TX, 19–21 April, 1983, 145–54.

[2]   MATHEW, J.–ALFREDSON, R. J.: The condition monitoring of rolling element bearings using vibration analysis. *Trans ASME, J Vibr, Acoust, Stress Reliab Design,* 106 (1984), 447–53.

[3]   DYER, D.–STEWART, R. M.: Detection of rolling element bearing damage by statistical vibration analysis. *Trans ASME, J Mech Design,* Vol. 100, No. 2 (1978), 229–235.

[4]   PATEL, J.–PATEL, V.–PATEL, A.: Fault Diagnostics of Rolling Bearing based on Improve Time and Frequency Domain Features using Artificial Neural Networks. *IJSRD,* Vol. 1, Issue 4, 2013.

APPLICATION OPTIONS OF ROLLER AND HYDROSTATIC BEARINGS IN MOTOR SPINDLES

SÁNDOR GERGŐ TÓTH–DÁNIEL TÓTH–GYÖRGY TAKÁCS

University of Miskolc, Department of Machine Tools
3515 Miskolc-Egyetemváros
tothsandorgeri@gmail.com; toth.daniel@uni-miskolc.hu; takacs.gyorgy@uni-miskolc.hu

Abstract: Due to higher requirements for accuracy appearing in machining, hydrostatic bearings have begun to be used in the motor spindles of high precision machine tools. These types of bearings have much better static stiffness and damping ratio, than rolling element bearings, but their rotational speed capability is strictly limited. This paper deals with the examination of hydrostatic bearings applications at high-speed machine tool spindles.

Keywords: hydrostatic bearings, damping capability, rotational speed

1. INTRODUCTION

Plain-bearing is one of the main variant of bearing technology. The surfaces of shaft and bearing slip on each other by the help of evolving oil film or grease, which are in accordance with the necessary requirements. Hydrostatic bearings pertain to the plain-bearings. In the hydrostatic bearings, the oil films are evolving by excess pressure developed by an external pump, so as to ensure the non-contact operation and load support capability. The main goal is that the flow rate must be nearly independent to loads, constantly. Under bearing loads, the clearances between shaft and inside bearing surface are changing too. To compensate this effect, orifices or capillaries must be maintained in front of the bearings recesses [1], [2].
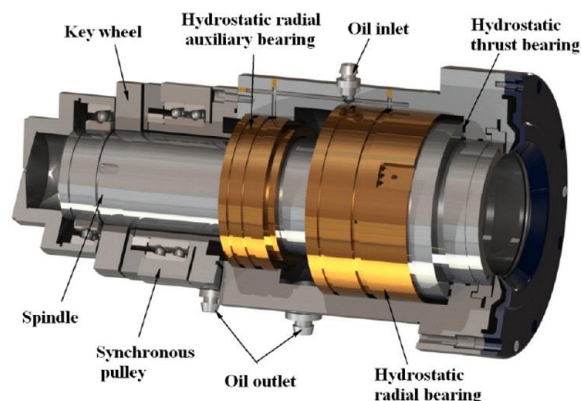

Figure 1. Motor spindle supported by hydrostatic bearings [3]

2. APPLICATIONS

These bearings are capable of the most support assignments, however due to expensive auxiliary arrangements, the economical operations are only potential, where ball bearings cannot be used and furthermore the fluid frictions are not provided by any other methods.

Moreover, hydrostatic bearings are widely mounted to high precision instruments and machine tools *(Figure 1)*. The main reason is, that the high bearing stiffness and low friction are primary requirements of these devices. Large-sized machines are also supported by hydrostatic bearings in case of the auxiliary arrangement's costs are much lower, than the machine price or the installation of ball bearings is uneconomical. The gradual application spreading is due to high stiffness and the significant damping capability are well combined, with which the surface roughness can be improved. The bearing design is almost optional: plain, spherical, cylinder and the combinations of these shapes can be chosen. The static stiffness and load support capability of hydrostatic bearings are independent from the fluid's viscosity (only from fluid pressure, and flow resistance at feed restrictor and the surface of oil film), so non-Newtonian fluids and gasses could be used [1], [2].

3. COMPARISON OF BALL AND HYDROSTATIC BEARINGS

In motor spindle applications, beside of the conventional ball bearings (steel or ceramic ball designs), most commonly hydrostatic bearing mountings are being used. So it is worth to make a comparison between these bearing designs in accordance with machining respects.

3.1. Load support and Stiffness

At hydrostatic bearings, the loads dissipate on a larger surface. That is why, compared with ball bearings (depends on the performance of external pump), these bearings support twice more. Their self-adjusting abilities derived from operating principle, so they are able to keep the original bearing centre-point. Moreover, in stable operating territory, load support capability does not depend on rotational speed loads *(not like hydrodynamic and rolling bearings, Figure 2).*

Figure 2. Bearing designs comparison in function to load capacity and rotational speed [5]
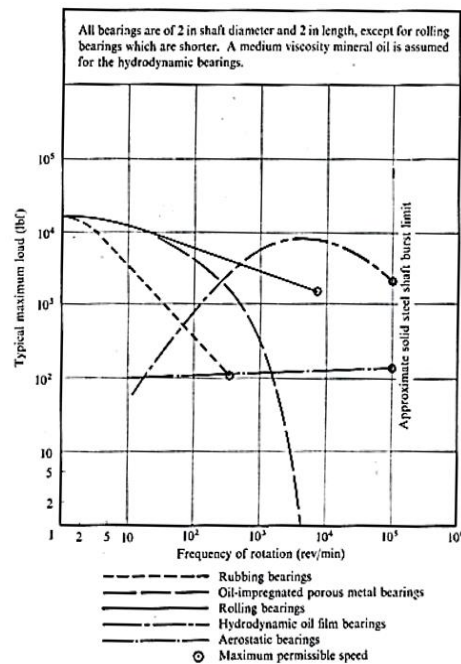
Ceramic balls have 50% larger modulus of elasticity, than steel balls, with that 20% larger rigidity can be reached, increasing the stiffness. In case of hydrostatic bearing, it can be achieved N/nm stiffness range and contact-deformation effects are not absent [4–6].

3.2. Accuracy and damping ratio

Ceramic balls have much better surface roughness, with that reducing the vibration and shaft swings. Accuracy of hydrostatic bearings depends on the manufacturing tolerances of bearing parts. Maximal rotational accuracy can be reached between 50 μm and 0,1 μm *(Figure 3)*.

Hybrid bearings has also better damping ratio than steel bearings. The thin oil film in hydrostatic bearings produces excellent damping in either directions: through compressibility of fluid film in normal direction and fluid shear rate at tangential direction. Damping ratio is particularly important coefficient, when the main goal is the manufacturing of really low surface roughness *(mirror surfaces)*. The productiveness can be improved, because the polishing operation could be negligible in most cases [4–6].
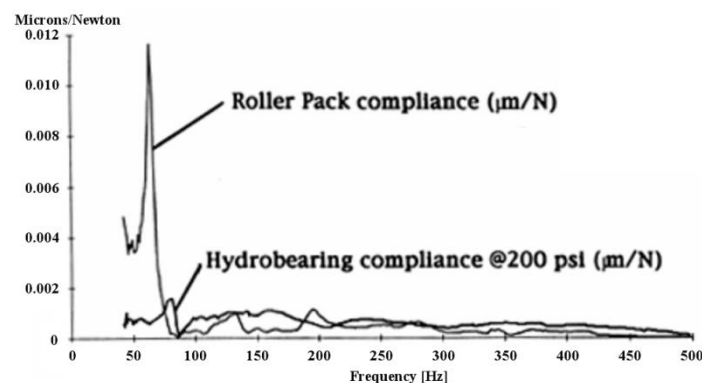

Figure 3. Comparison of bearing compliances at 200 psi ≈ 14 bar, in function to frequencies [8]

3.3. Friction and thermal properties

Though by using hybrid ceramic bearings, the coefficient of friction and channelling effect can be reduced, these bearings have strictly limited service life. On the other hand, due to parts in the hydrostatic bearings slip on each other through a fluid film, friction is nearly zero and wear will not occur.

At ball bearings, due to heat produced by friction, additional external cool and lubrication systems need to be installed. Because of fluid pressure, energy is induced into the hydrostatic bearing. The oil oozes out slowly from the bearing into a drip pan. In the pan, the pressure and flow rate are nearly zero, so all initial energy turns into fluid shear. This energy dissipates as heat. The rise in temperature

of oil also depends on heat produced by the machine. With this effect taking into account, it is worth using the possibly lowest pressure and flow rate at hydrostatic bearings. The fluid shear also generates heat in the bearing clearances at high speeds [4–6].

3.4. Rotational speed

By hydrostatic bearings only fluid friction are developing in fluid films during movement. In this case, the flow is laminar. However, at high speeds hydrodynamics effects occur, which tend to change the flow from laminar to turbulent. This occurrence leads to vibrations and shaft deflections, that finally results total bearing failure. For compensating this disadvantage, several research has made so far. With patterned *(ribbed)* internal bearing surfaces, the dynamic stiffness can be improved. Moreover, using of non-Newtonian fluids *(electro- and magnetic-rheological fluids)* results better controllable real-time balance [7].

Table 1
Maximal speed capabilities at different bearing designs [5]

Bearing type	Estimated maximum speed (dN factor)
Steel ball bearings	1 000 000
Ceramic ball bearings	2 000 000
Hydrostatic bearings	1 000 000

The table shows the achievable maximum speed capabilities of different bearing designs. For the characterization of speeds, dN factor is prefer being used, because the bearing rotational speed (*N- 1/min)* significantly connects with its diameter *(d- mm).* The allowable rotational speed of steel ball bearings are nearly equal to the hydrostatic bearings. The density of ceramic balls is only 40% of those in conventional steel bearings. If hybrid ceramic bearings are installed in motor spindle, then the centrifugal force will be reduced at the adjusted preload, so this bearing design are highly recommended at high-speed applications [4–6].

3.5. Reliability and costs

Roller bearings have limited service life, the long term collapse is typically output by bearing runway fatigue or the termination of appropriate lubrication. The bearing life time is being significantly reduced if the operating temperature rises or the machine load is too high. The roller bearings are especially sensitive to the contaminations, so the assembly must be performed in the possible cleanest environment. During operating, labyrinth seals and air-cleaner instruments are usually adopted to prevent the cooling and cutting wastes getting into the bearing. The lubrication effect of ball bearings, exposed to humid environment for a long time, greatly deteriorates in case of grease lubrication. Machine collisions usually cause bearing runway deformations *(brinelling),* if the loads are heavy during

impact. Most parts of roller bearings rotate at high speeds, which can generate noise during specific environment. The noisy spindle is the result of bearing malfunctions, in such cases the bearing replacement must be performed as soon as possible.

The features of hybrids bearings assist to reducing wear, meanwhile improving corrosion-resistance and lubrication life. In addition to high service life, lower vibration state and noise level can be reached with silicon-nitride balls.
Hydrostatic bearings are non-contact bearings, so they have infinite service life in theory. However, during operations the appropriate filtration of lubrication fluid is indispensable. The fluid constantly flows from gaps, thus greatly prevent to get contaminations into hydrostatic bearings. Most cases, the part is closed hermetically so as to estop of the lubrication fluid pollution. If the sealing is damaged and polluted by coolant, then the lubrication oil must be exchanged periodically.

The parts of high precision ball spindles have strictly geometric tolerances *(0,002–0,003 mm shaft diameter tolerances)* which cause higher manufacturing cost. Installation of these bearings requires highly skilled workmen and additional mounting costs *(parts heating for fitting)*. Ball bearings are very sensitive to contaminations: the installation and operating environment must be clean. Supporting optimal operating, bearings must be chilled and lubricated by auxiliary equipment. Newly installed roller elements of ball bearings with grease lubrication must be run in protractedly and carefully. In the course of the gradual increase of spindle rotational speed, grease can distribute properly among roller elements in the bearing *(Figure 3)*. Due to higher prime costs, hybrid bearings were not able to spread widely, but owing to different manufacturing improvements, their purchase prices are much lower nowadays.
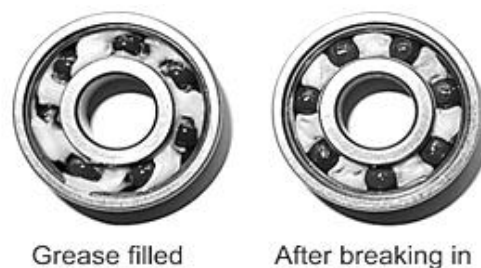

Grease filled   After breaking in

Figure 4. State of the hybrid bearings lubrication before and after breaking in [9]

On the other hand, tolerances of hydrostatic bearings are significantly higher. Because of the simple construction, the installation into the motor spindle requires less time. The lower tolerances cause higher clearances between the shaft and internal bearing ring, so heating is not necessary at mounting. Because of hydrostatic bearing features, the maintenance cycles are fewer, and take less time against ball bearings. The main operating costs are derived from the auxiliary

equipment: external pump, filters, valves, cooling units, pressure switches as well as hydraulic tanks and batteries. The maintenance of these instruments must be regular, because of their limited service lives [4–6].

4. CONCLUSION

The application of hydrostatic bearings could replace ball bearings in motor spindles, however the rotational speed limitation, derived from turbulent flow, does not allow widely. It is worth making additional researches because they have excellent damping capabilities which are necessary for high precision machining. A turbulent flow model should be set up to examine the hydrodynamic phenomena. Moreover, the application of controllable fluids could be considered to reach better real-time balance.

REFERENCES

[1] SAN ANDRÉS, Luis: *Hydrostatic Journal Bearings,* Texas A&M University, 2009.

[2] MÖRK, J.–MOLNÁR, L.–LUGOSI, L.: *Hidrosztatikus csapágyak méretezésének elvi alapjai.* Miskolci Egyetem, 1990.

[3] HE, Qiang–LI, Lili–REN, Fengzhang–VOLINSKY, Alex: Numerical Simulation and Experimental Study of the Hydrostatic Spindle with Orifice Restrictors. *The Open Mechanical Engineering Journal,* Vol. 10, 2016.

[4] SKF: *High precision hybrid bearings for increased spindle performance.* Dd 7817/II E. Sweden, 1996.

[5] XIE, Xiaofan: *Comparison of Bearings.* University of Utah, 2012.

[6] WASSON, Kevin L.: *A Comparison of Rolling Element and Hydrostatic Bearing Spindles for Precision Machine Tool Applications Hardinge.* Inc. Elmira, Ny USA, NA.

[7] OCHONSKI, W.: *The attraction of ferrofluid bearings.* Univ. of Mining and Metallurgy, Krakow, 2005.

[8] SRINIVASAN, V.: Analysis of Dynamic Load Characteristics on Hydrostatic Bearing with Variable Viscosity and Temperature using Simulation Technique. *Indian Journal of Science and Technology,* Vol. 6, 2013, 6.

[9] http://www.vcrcbike.com/articles.asp?id=157

REVIEWING COMMITTEE

PUBLICATION OF THE UNIVERSITY OF MISKOLC – A SHORT HISTORY

The University of Miskolc (Hungary) was founded by the Empress Maria Teresia in Selmecbánya in 1735. After the first World War the university moved to Sopron, where in 1929, it started the series of university publications with the title *Publications of the Mining and Metallurgical Division of the Hungarian Academy of Mining and Forestry Engineering* (Volumes I–VI). From 1934 to 1947 the Institution became the Faculty of Mining, Metallurgical and Forestry Engineering of the József Nádor University of Technology and Economical Sciences at Sopron. The publications got the title *Publications of the Mining and Metallurgical Engineering Division* (Volumes VII–XVI). For the last volume before 1950 – due to a further change in the name of the Institution – Technical University, Faculties of Mining, Metallurgical and Forestry Engineering, *Publications of the Mining and Metallurgical Division* was the title. For some years after 1950 the Publications were temporarily suspended. After the foundation of the Mechanical Engineering Faculty in Miskolc in 1949 and the movement of the Sopron Mining and Metallurgical Faculties to Miskolc the Publications restarted with the general title *Publications of the Technical University of Heavy Industry* in 1955. Four new series – Series A *(Mining),* Series B *(Metallurgy),* Series C *(Machinery)* and Series D *(Natural Sciences)* – were founded in 1976. These came out both in foreign languages (English, German and Russian) and in Hungarian. In 1990, right after the foundation of some new faculties, the university was renamed to University of Miskolc. At the same time the structure of the Publications was reorganized so that it could follow the faculty structure. Accordingly three new series were established: Series E *(Legal Sciences),* Series F *(Economical Sciences)* and Series G *(Humanities and Social Sciences).* The latest series, the Series H *(European Integration Studies)* was founded in 2002. *Design of Machines and Structures* (**HU ISSN 1785-6892(Print), HU ISSN 2064-7522(Online)**) first published in 2003 as a part of the Series C.